Protein structure and dynamics by NMR

Otten, Renee

Chapter 2

Iron Transport in *Escherichia coli*: NMR Studies of the Periplasmic Binding Protein FepB

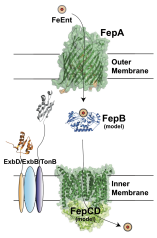

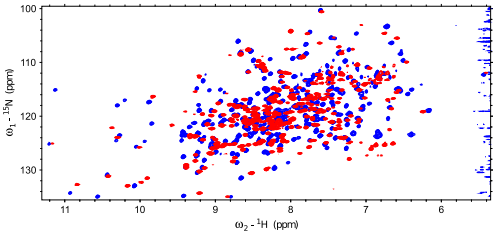

Renee Otten[1], Byron Chu[2], Hans J. Vogel[2] and Frans A. A. Mulder[1]

[1] Groningen Biomolecular Sciences and Biotechnology Institute (GBB), University of Groningen, Nijenborgh 4, 9747 AG Groningen, The Netherlands

[2] Biochemistry Research Group, Department of Biological Sciences, University of Calgary, 2500 University Drive Northwest, Calgary, Alberta T2N 1N4, Canada

2.1 Abstract

An NMR study of both the apo- and holo-state of FepB, a periplasmic binding protein (PBP) involved in iron uptake in *E. coli*, is described. For both forms of this 34 kDa protein, a nearly complete backbone and methyl group assignment was obtained. The analysis of the assigned chemical shifts indicates that FepB has a mixed alpha-helical/beta-strand topology with a central alpha-helix, similar to the PBPs in cluster A. Binding of the negatively charged gallium enterobactin ligand causes extensive chemical shift perturbations for all nuclei, but the overall topology of the protein remains similar. Most significant changes are observed in the C-terminal part of the protein, where there is a transition from coil to beta-strand for residues 227–242 and from alpha-helical to more extended for residues 294–302. ^{15}N backbone relaxation data indicate that FepB is a rather well ordered protein both in the absence and presence of the ligand, with the exception of the first 25 N-terminal residues which are highly flexible. However, in the ligand-free state of FepB there is significantly more mobility observed for the region between residues 225–250, consistent with the absence of a stable secondary structure element. Ligand binding largely suppresses this dynamics and is consistent with a transition from coil to beta-strand for this part of the protein. With the currently available NMR data we can neither discriminate between the suggested binding modes for PBPs (i.e., "Venus flytrap", hardly any conformational changes, or mainly involvement of loops) nor shed light on the reason for the ligand specificity. High-resolution structures of the ligand-free (apo) and ligand-bound (holo) states of FepB are required to answer these questions and research toward this goal is currently pursued in our laboratories.

2.2 Introduction

Iron is an essential nutrient for almost every microorganism due to its diverse role in the biochemistry of the cell (e.g., as redox center in electron carriers or co-factor for enzymes, and as regulator in cellular biosynthesis and metabolism). Despite the fact that iron is the most abundant transition metal on earth, bacteria face difficulties to keep their internal concentration above the required $\sim 10^{-6}$ M. The relevant species of iron available for cellular uptake are ferrous iron (Fe^{2+}) and ferric iron (Fe^{3+}). Ferrous iron is highly soluble in aqueous solutions at neutral

pH and can be imported by pervasive divalent metal transporters. However, in most environments, except for anaerobic or low pH conditions, it is impossible to maintain this reductive state and ferrous iron is quickly oxidized to ferric iron. The bio-availability of iron is, therefore, governed by the (in)solubility of Fe^{3+} around pH 7 and is limited to $\sim 10^{-18}$ M (Raymond & Carrano, 1979). The situation is even more challenging in mammalian hosts, where the strict iron homeostasis leads to a free iron concentration in the serum of $\sim 10^{-24}$ M (Aisen et al., 1978; Martin et al., 1987; Kretchmar et al., 1988). Moreover, even at these low concentrations free ferric and ferrous iron are highly toxic to the cell, in the case of Fe^{2+} due to the formation of radicals in Fenton or Haber–Weiss reactions (Braun, 1997; Touati, 2000). The limited availability and toxicity together with the biological imperatives ensured that microorganisms, including pathogens, have evolved a variety of high-affinity iron acquisition and transport systems (Clarke et al., 2001; Faraldo-Gómez & Sansom, 2003; Krewulak & Vogel, 2008; Chu et al., 2010).

Bacteria and fungi, for example, produce and secrete small organic compounds in response to iron-stress that are capable of liberating the iron from its organic or inorganic complexes. These so-called siderophores (from the Greek: "iron carriers") have been divided in three major groups, depending on the chemical nature of the ligands: catecholates (e.g., enterobactin), hydroxamates (e.g., ferrichrome), and α-hydroxy-carboxylates (e.g., staphyloferrin A) (Miethke & Marahiel, 2007). Various siderophores contain more types of functional groups coordinating to the metal ion and are, therefore, classified as "mixed-type" siderophores. In general, siderophores form a hexadentate complex with the iron that cannot enter the bacterial cell through passive diffusion, due to its low concentration and large dimensions ($M_w \sim 750$ Da). Therefore, active transport is necessary to shuttle the ferric-siderophore complex from the extracellular fluid across the membrane(s) into the cytosol. In Gram-positive bacteria, the uptake of the iron complex is mediated by a membrane-anchored binding protein and a membrane-associated ATP-binding cassette (ABC) transporter. In Gram-negative bacteria (e.g., *Escherichia coli*) the situation is more complex because these organisms have an additional double-layered lipid membrane. The outer membrane (OM) affords further protection to the environment, but at the same time poses another barrier for the uptake of the iron-siderophore complex (Postle, 1990). Ions and other small molecules can diffuse passively across the OM by taking advantage of pore-forming proteins known as porins (Koebnik et al., 2000), but siderophores are unable to use this route and do rely on active transport. All uptake pathways in Gram-negative bacteria require,

therefore, an outer membrane transporter besides a periplasmic binding protein (PBP, *cf.* the membrane-anchored binding protein in Gram-positive bacteria) and the inner membrane (IM) ABC transporter. The energy for the active transport across the OM is supplied through coupling of the proton motive force (PMF) of the cytoplasmic membrane to the outer membrane via the TonB complex (Moeck & Coulton, 1998).

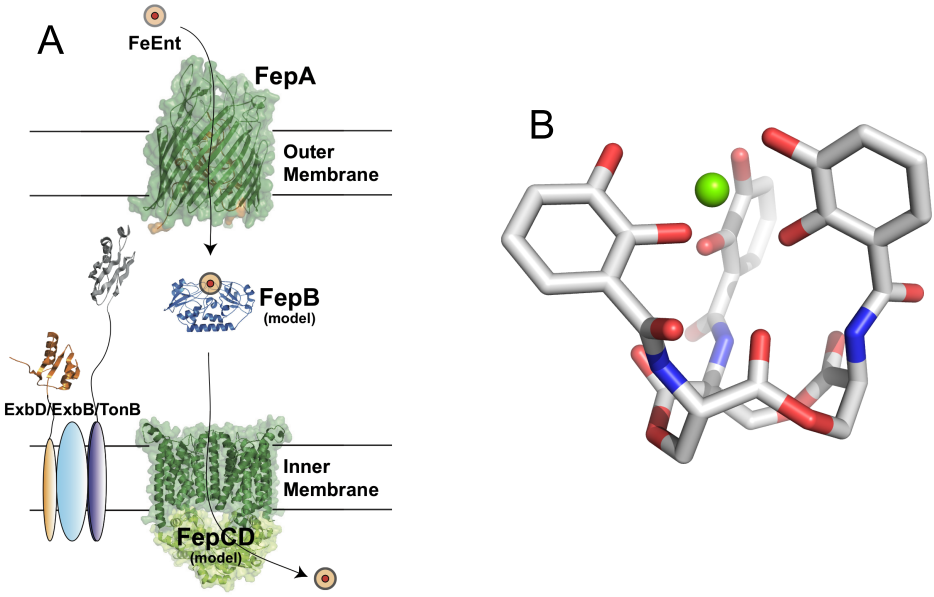

Figure 2.1. Schematic overview of the ferric enterobactin transport system of *E. coli* (panel A) and the structure of the negatively (3–) charged ferric enterobactin complex (panel B). Panel A is reprinted with kind permission from Springer Science + Business Media: Biometals (Chu et al., 2010), copyright (2010).

Iron uptake systems are present in *E. coli* for the uptake of both Fe^{2+} and Fe^{3+}. Fe^{2+} transport is mediated by porins across the OM and the Feo system (Kammler et al., 1993) across the IM, while Fe^{3+} uptake exploits the following three TonB complex dependent systems: Fhu (ferric-hydroxamate), Fep (ferric-catecholate), and Fec (ferric di-citrate). The ferric enterobactin (FeEnt) transport system is shown schematically in Figure 2.1 (scheme A), where the unknown structures of FepB and FepCD are represented by holo-BtuF (1N4A) and BtuCD (1L7V), respectively. Enterobactin is a small (669 Da) organic molecule of the catecholate-type siderophore (Figure 2.1, scheme B) synthesized by *E. coli* and *S. typhimurium*,

but utilized by all Gram-negative enteric bacteria (Raymond et al., 2003) and its biosynthesis is strictly controlled by the Fur (Ferric uptake regulation) protein (Hantke, 2001). Of note, while *E. coli* only synthesizes and secretes enterobactin, it is able to scavenge different siderophores produced by other organisms. High-affinity binding of iron by enterobactin takes place through a right-handed (Δ) coordination propeller of the catechol rings around the metal ion (Raymond et al., 2003) with a formal stability constant, K_f, of 10^{49} (Loomis & Raymond, 1991) and yields a FeEnt complex with a net charge of –3 (Lee et al., 1985). The outer membrane receptor, FepA, mediates the initial, rate-limiting, uptake of ferric enterobactin (K_d $\sim$0.1 nM (Newton et al., 1999)) and its structure has been solved by X-ray crystallography (Buchanan et al., 1999). Consistent with other OM proteins, the topology consists of a 22-stranded anti-parallel β-barrel spanning the membrane connected with a few large, extracellular loops. Additionally, the N-terminal part of the membrane protein ($\sim$160 residues) folds independently into a globular domain (termed the "cork") that occludes the interior of the β-barrel. Both the cluster of extracellular loops and the "cork" domain are implicated to contribute to the ligand binding pocket and binding specificity and affinity. The uptake of ferric enterobactin by FepA is accompanied by a conformational rearrangement of the N-terminal domain and the energy for this process is supplied by the TonB complex (TonB-ExbBD) (Moeck & Coulton, 1998). Once transported across the OM, FeEnt is transferred by the periplasmic binding protein FepB (K_d $\sim$30 nM (Sprencel et al., 2000)) to the ATP-binding-cassette (ABC) transporter, FepCDG, in the inner membrane. The proteins FepD and FepG together form the cytoplasmic pore, while FepC functions as the cytoplasmic ATPase, providing the energy needed for the uptake of FeEnt. As a final step, the intracellular release of iron is most likely achieved either by reduction of Fe^{3+} to Fe^{2+} or the hydrolytic cleavage of the backbone of ferric enterobactin by FeEnt esterase, encoded by the *fes* gene (Brickman & McIntosh, 1992).

FepB belongs to a large family of structural related PBPs, which are essential in solute uptake (Boos & Lucht, 1996). PBPs recognize a broad spectrum of substrates including sugars, amino acids, peptides, various ions, and vitamins (Higgins, 1992; Berntsson et al., 2010). Due to this wide variety of ligands, PBPs are mostly unrelated at the level of primary sequence (diverse sequences and length), but, nevertheless, show remarkably conserved structural features. All PBPs consist of two independent, folded globular domains (mixed α/β, Rossmann-like fold) connected by a hinge-region. PBPs have been clustered based on similarities in

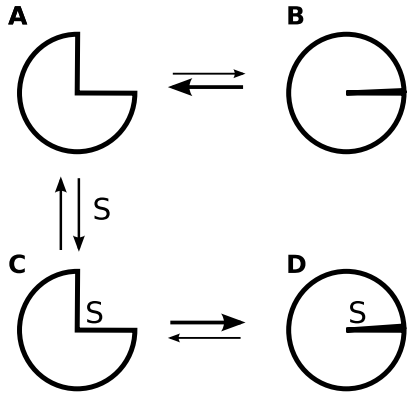

Figure 2.2. Schematic overview of the different states in the "Venus flytrap" binding mechanism of PBPs. The conformations (A: "open-unliganded"; B: "closed-unliganded"; C: "open-liganded"; D: "closed-liganded") are in kinetic equilibrium. In the absence of a ligand the equilibrium is highly skewed toward conformation A, and upon ligand binding the equilibrium shifts toward conformation D. Reprinted with permission from Berntsson et al. (2010).

primary sequence (9 clusters) (Tam & Saier, 1993; Claverys, 2001; Krewulak et al., 2004), the topological arrangement of secondary structure elements in the globular domains (Fukami-Kobayashi et al., 1999; Berntsson et al., 2010), and the number of interdomain connections (3 groups) (Quiocho & Ledvina, 1996; Lee et al., 1999). We will follow here the recently published, structural classification by Berntsson and co-workers, which divides the PBPs in six different clusters (Berntsson et al., 2010). Cluster A (group III) consists of PBPs that have one, α-helical, interdomain connection, while clusters B (group I) and C–F (group II) are connected by three and two β-strands, respectively.

Ligand binding takes place in a cleft between the two domains, which is accessible in the "open-unliganded" conformation (Figure 2.2, conformation A). Domain closure occurs upon substrate binding in a so-called "Venus flytrap" or "Pac-man" motion, and the ligand is trapped at the interface between the two domains ("closed-liganded conformation"; Figure 2.2, conformation D) (Mao et al., 1982). Mounting evidence shows that the open and closed forms are in kinetic equilibrium (Walmsley et al., 1992; Oh et al., 1993; Flocco & Mowbray, 1994; Wolf et al., 1994; Ledvina et al., 1998; Björkman & Mowbray, 1998; Tang et al., 2007), and also suggests that "closed-unliganded" and "open-liganded" states are populated (see Figure 2.2, conformations B and C). In the absence of ligand (apo-state), the protein is assumed to be flexible and mainly in the "open-unliganded" conformation, while ligand binding (holo-state) that involves residues on both domains shifts the equilibrium toward the "closed-liganded" state. However, the conformational change upon ligand binding (i.e., the amount of closing of the two domains) varies

dramatically between PBPs from the different structural clusters. Large rigid body domain reorientation is observed for PBPs in clusters B–F (e.g., $\sim$35° for maltose binding protein (Sharff et al., 1992; Quiocho et al., 1997)), but the conformational changes vary significantly for PBPs in cluster A. Some systems (e.g., FitE (Shi et al., 2009), FeuA (Peuckert et al., 2009), and HmuT (Mattle et al., 2010)) undergo large, hinged motions similar to what is observed for PBPs in clusters B–F. On the other hand, FhuD (Clarke et al., 2000, 2002; Krewulak et al., 2005; Krewulak, 2005), FhuD1 and FhuD2 (Sebulsky et al., 2003, 2004) show only modest interdomain motion and for other systems (e.g., BtuF (Borths et al., 2002; Karpowich et al., 2003), ShuT and PhuT (Ho et al., 2007), ZnuA (Yatsunyk et al., 2008), and TroA (Lee et al., 1999, 2002)) the apo- and holo-forms are almost identical.

As discussed above, the exact binding mode of PBPs with a central α-helix as hinge region (cluster A) remains elusive as high-resolution structures suggest different possibilities. It is, however, important to realize that all this information is deduced from the comparison of crystal structures. It is, therefore, plausible that crystal packing significantly affects the observed degree of opening and is thus not representative for the situation in solution. The disagreement between the degree of opening in the X-ray and NMR structures of β-cyclodextrin bound to maltose binding protein (MBP), 2.8 versus 12.8 degrees, is a clear indication of this potential issue (Evenäs et al., 2001). Furthermore, it should be noted that molecular dynamics (MD) simulations on BtuF (Kandt et al., 2006; Liu et al., 2008b), ShuT and PhuT (Liu et al., 2008a) indicate that the structural changes upon ligand binding might be more pronounced than anticipated from the crystal structures.

We, therefore, decided to study the periplasmic binding protein FepB, which is predicted to fall in cluster A, in both the apo- and holo-state using Nuclear Magnetic Resonance (NMR) spectroscopy and investigate the effect of ligand binding on its secondary structure and dynamics. Besides trying to shed some light on the binding mode of this group of PBPs, FepB is also an interesting system due to the fact that the binding affinity for its ligand (K_d in the nM range) is an order of magnitude higher than for most other PBPs. Moreover, FepB selectively binds enterobactin while similar catecholate-type siderophores as vibriobactin (Wyckoff et al., 1999) and agrobactin (Sprencel et al., 2000) are not recognized. To answer questions on ligand binding and specificity as raised above, high-resolution structures of the "open-unliganded" (apo) and "closed-liganded" (holo) states are needed together with knowledge about protein dynamics.

Our NMR studies on FepB yielded nearly complete backbone and methyl group assignments for both the apo- and holo-state. From the assigned chemical shifts it was shown that the protein has a mixed α/β topology with a central α-helix, consistent with PBPs in cluster A. The binding of the negatively charged gallium enterobactin ligand causes significant chemical shift perturbations, but the overall topology of the protein remains similar. ^{15}N backbone relaxation data indicate that both apo- and holo-FepB are well ordered, with the exception of the first 25 N-terminal residues. Moreover, in apo-FepB there is a significant mobile region observed between residues 225–250, while the dynamics for this region is largely suppressed upon ligand binding. However, to determine the exact binding mode of FepB and its ligand, additional structural data (e.g., RDCs and NOEs) is required and research along these lines is currently pursued.

2.3 Materials and Methods

2.3.1 Sample Preparation

Mature *fepB* (Elkins & Earhart, 1989) with the signal sequence removed was cloned into pET-19b (Novagen) to generate plasmid pFepB (Krewulak, 2005). *E. coli* BL21(DE3) was used to express recombinant FepB with an N-terminal 10xHis tag (315 residues, ∼34 kDa). For the induction of protein synthesis, cells were grown at 37 °C in M9 minimal medium with 100 μg/mL ampicillin to an $OD_{600} \approx 0.8$ and incubated for 3 h at the same temperature in the presence of 0.5 mM isopropyl β-D-thiogalactoside (IPTG). To purify FepB, cell pellets were resuspended in a buffer containing 20 mM Tris-HCl, pH 8.0, and 500 mM NaCl with 10 μg/mL DNAse I and 0.5 mM phenylmethanesulfonyl fluoride (PMSF) added. After French press (SLM-Aminco/Spectronic), the cell lysate was loaded onto a nickel Sepharose column (GE Healthcare) pre-equilibrated with 20 mM Tris-HCl, pH 8.0, and 500 mM NaCl. After extensive washing, FepB was eluted with 20 mM Tris-HCl, pH 8.0, 500 mM NaCl, and 200 mM imidazole, and homogeneity was confirmed by 15% SDS-PAGE.

A U-[^{13}C,^{15}N]-^{1}H/^{2}H sample of FepB was obtained using the general isotope labeling-strategy outlined by Tugarinov et al. (2006). Briefly, pFepB – *E. coli* BL21(DE3) was grown in 1 L of D_2O M9 medium containing 3 g/L U-[^{1}H,^{13}C]-D-glucose (Cambridge Isotope Laboratories) and 1 g/L $^{15}NH_4Cl$ (Cambridge Isotope Laboratories) as the sole carbon and nitrogen sources, respectively. M9 medium

initially contained 90 nM $FeCl_2$, and additional supplementation with $FeCl_2$ (300 nM final concentration) was required to suppress native enterobactin production. A second NMR sample for the stereospecific assignment of methyl groups was prepared using 10% U-[^{1}H,^{13}C]-D-glucose and 90% unlabeled glucose as described earlier by Neri et al. (1989), but growth was performed in 100% D_2O. A third U-[^{15}N]-^{1}H/^{2}H sample of FepB was prepared to perform ^{15}N relaxation studies.

A U-[^{13}C,^{15}N]-^{1}H/^{2}H FepB sample loaded with Ga^{3+}–enterobactin was prepared using iron-free enterobactin obtained from Professor G. Winkelmann (University of Tübingen). A 10 mM Ga^{3+}–enterobactin stock solution (1 mg of iron-free enterobactin dissolved in 10 mM Ga_3NO_4, 20 mM Tris-HCl, pH 8, 33 v/v% methanol) was prepared and titrated into the protein solution until the [^{1}H$-^{15}$N]-HSQC spectrum did not change anymore. Complete removal of the methanol by extensive dilution-concentration steps and freeze-drying of the sample was confirmed by 1D ^{1}H NMR (data not shown).

All NMR samples contained $\sim$1 mM FepB, and 50 mM sodium phosphate, pH 6.4 (93% H_2O and 7% D_2O).

2.3.2 NMR Spectroscopy

NMR experiments were performed at 25 °C on a Varian Unity Inova (600 and 800 MHz) or Bruker Avance 700 MHz four-channel spectrometer, equipped with a triple-resonance room temperature (600 and 800 MHz) or cryogenically cooled (700 MHz) probehead with pulsed field gradient capabilities.

NMR Chemical Shift Assignment

Sequential backbone assignments were obtained by recording a series of TROSY (Pervushin et al., 1997) variants of the standard experiments on a 600 (apo-FepB) or 700 MHz (holo-FepB) spectrometer.

Chemical shift assignments for apo-FepB were obtained by recording 3D CT-HNCA, CT-HN(CO)CA, HN(CA)CB, HN(COCA)CB, HN(CA)CO, and HNCO experiments (Yang & Kay, 1999b); a 3D ^{15}N-edited NOESY-HSQC (Marion et al., 1989) and 4D HN$CO_{i-1}CA_i$ (Konrat et al., 1999) were recorded to confirm the assignments. Chemical shift assignments for holo-FepB were obtained by recording 3D HNCA, HN(CO)CA, HNCACB, HN(CO)CACB, HN(CA)CO, and HNCO

experiments (Salzmann et al., 1998, 1999; Eletsky et al., 2001).

Side chain assignments of methyl-containing amino acids for both systems were obtained using the 3D C-TOCSY-CHD_2 experiment on the same U-[^{13}C,^{15}N]-^{1}H/^{2}H labeled protein sample as described earlier (Otten et al., 2010) (see Chapter 3). Stereospecific assignments for Leu and Val residues were obtained from a CHD_2-detected CT-[^{1}H$-^{13}$C]-HSQC spectrum acquired on the 10% ^{13}C-labeled sample of apo-FepB on the basis of the sign of the cross-peaks relative to the ϵ-methyl group of Met. Stereospecific assignments for holo-FepB were not determined experimentally, but inferred from the comparison of the apo- and holo-FepB spectra.

See the Appendix, Table A2.1, for a detailed description of the experimental parameters and Tables A2.3 and A2.4 for the chemical shift assignments of apo-FepB and holo-FepB, respectively.

NMR Spin Relaxation Measurements

All spin relaxation experiments for apo-FepB were conducted at two static magnetic field strengths (600 and 800 MHz). The backbone ^{15}N relaxation experiments (R_1, $R_{1\rho}$, and {^{1}H}-^{15}N NOE) were recorded on the U-[^{15}N]-^{1}H/^{2}H labeled sample using TROSY-modified versions of the experimental schemes described by Farrow et al. (1994) and Akke & Palmer (1996). R_1 values were measured from 16 (600 MHz) or 14 (800 MHz) 2D spectra recorded in an interleaved fashion, with T delays of 0, 125.24, 250.48, 375.72, 500.96, 751.44, 1001.92, 1252.40 (2x), 1502.88 (2x), 1753.36 (2x), and 2003.84 (3x) ms (600 MHz) or 0, 276.73, 415.10, 553.46, 830.19, 1106.92, 1383.65 (2x), 1660.38, 1937.11 (2x), and 2213.84 (3x) ms (800 MHz). $R_{1\rho}$ values were measured from 15 2D spectra recorded in an interleaved fashion, with T delays of 0, 6, 12, 18, 24, 30 (2x), 36 (2x), 42 (2x), 48 (2x), and 54 (2x) ms using a 1.7 (600 MHz) and 2.0 (800 MHz) kHz spin-lock field. {^{1}H}-^{15}N NOE experiments were recorded with (NOE) and without (REF) a ^{1}H pre-saturation period of 3 seconds and an interscan delay of 10 s (600 MHz) or 11 s (800 MHz) was used for both experiments.

All spin relaxation experiments for holo-FepB were conducted at a single static magnetic field strength (700 MHz). The backbone ^{15}N relaxation experiments (R_1, R_2, and {^{1}H}-^{15}N NOE) were recorded on the U-[^{15}N,^{13}C]-^{1}H/^{2}H labeled sample using the experimental schemes described by Zhu et al. (2000). R_1 values were measured from 12 2D spectra recorded in an interleaved fashion, with T delays of 100, 170, 400 (2x), 680, 850, 1010, 1250, 1500 (2x), 1700, and 2000 ms. R_2 values were

measured from 12 2D spectra recorded in an interleaved fashion, with T delays of 16 (2x), 32 (2x), 48 (2x), 64 (2x), 80 (2x), and 96 (2x) ms. $\{^1H\}$-^{15}N NOE experiments were recorded with (NOE) and without (REF) a ^1H pre-saturation period of 5 seconds and an interscan delay of 5 seconds was used for both experiments.

See the Appendix (Table A2.2), for a detailed description of the experimental parameters to measure the relaxation parameters of apo-FepB and holo-FepB.

2.3.3 Data Processing and Analysis

All data sets were processed with the NMRPipe/NMRDraw software package (Delaglio et al., 1995) and analyzed using the program Sparky (Goddard & Kneller, 2008). Briefly, an appropriate linear prediction algorithm (mirror image linear prediction (Zhu & Bax, 1990) for constant-time evolution or forward-backward linear prediction (Zhu & Bax, 1992) in the case of real-time evolution) was employed to double the indirect domains. A cosine-squared window function was employed in all domains. All chemical shifts are referenced to DSS according to Wishart et al. (1995b).

The values of R_1, $R_{1\rho}$, and R_2 were obtained by fitting the extracted cross-peak intensities to a mono-exponential decay. Intensities were extracted using the program Sparky (Goddard & Kneller, 2008) and data fitting was performed using Curvefit v1.4 (http://www.palmer.hs.columbia.edu/software/curvefit.html) using the script "sparky2rate" (http://xbeams.chem.yale.edu/ loria/sparky2rate). Uncertainties in the peak heights were determined from duplicate measurements and uncertainties in the longitudinal and transverse relaxation rates were estimated from Jackknife simulations (Mosteller & Tukey, 1977). In the case of apo-FepB, R_2 values were calculated from $R_{1\rho}$ values corrected for resonance offset effects (Peng & Wagner, 1992), using the following relationship:

$$R_{1\rho} = R_1 \cdot \cos^2\theta + R_2 \cdot \sin^2\theta$$

where $\theta = \tan^{-1}(\nu_1/\Delta\nu)$, ν_1 is the spin-lock frequency and $\Delta\nu$ is the difference between ^{15}N offset frequency and the ^{15}N carrier frequency. $\{^1H\}$-^{15}N NOE values were determined from the experiments with and without irradiation and their uncertainty was estimated from the root-mean-square of the noise level. For some residues the signal intensity was rather low, resulting in a high(er) uncertainty in

the R_1, R_2, and $\{^1H\}$-^{15}N NOE values. Data points for which the relative error was larger than 25% were excluded from the analysis.

An analysis of secondary structure elements on the basis of $^1H^N$, ^{15}N, $^{13}C'$, $^{13}C^\alpha$, and $^{13}C^\beta$ chemical shifts was performed using the **n**eighbor **c**orrected **S**tructural **P**ropensity **C**alculator (ncSPC) (Tamiola et al., unpublished results), available as a web-server (http://www.protein-nmr.org). The analysis was performed with the random coil chemical shift library described by Tamiola et al. (2010) using the assigned chemical shift data for the above-mentioned nuclei as input for the calculations, and the raw output data (without moving average) was used in the analysis.

The protein flexibility was predicted from the chemical shifts, based on the "random coil index" as proposed by Berjanskii & Wishart (2005) using the webserver available at http://wishart.biology.ualberta.ca/rci.

Absolute chemical shift changes upon ligand-binding were compared on a per-residue basis for all backbone resonances and methyl groups individually. Furthermore, a combined chemical shift change per residue was calculated for backbone and methyl resonances by combining all chemical shifts:

$$\Delta\delta_{bb} = \sqrt{(\Delta\delta_{H^N})^2 + (\Delta\delta_N / R_N)^2 + (\Delta\delta_{C'} / R_{C'})^2 + (\Delta\delta_{C^\alpha} / R_{C^\alpha})^2 + (\Delta\delta_{C^\beta} / R_{C^\beta})^2}$$

$$\Delta\delta_{methyl} = \sqrt{(\Delta\delta_{H^M})^2 + (\Delta\delta_{C^M} / R_{C^M})^2}$$

where R_i denotes the scaling factor of nucleus i and these were determined according to Mulder et al. (1999) from the ratio of the average standard deviations, $< \sigma_\delta >_i$ / $< \sigma_\delta >_{H^N}$ for backbone nuclei and $< \sigma_\delta >_i$ / $< \sigma_\delta >_{H^M}$ for methyl groups. Using the chemical shift data available in the BioMagResBank (http://bmrb.wisc.edu) for the 20 common amino acids in proteins we obtained the following scaling factors: R_N = 6.4, $R_{C'}$ = 3.0, R_{C^α} = 3.5, R_{C^β} = 3.2 and R_{C^M} = 5.4.

Corrections for deuterium isotope effects were done for ^{15}N, $^{13}C^\alpha$, and $^{13}C^\beta$ chemical shifts (Venters et al., 1996; Gardner et al., 1997) prior to chemical shift analysis. It should be noted, however, that these isotope corrections were determined for perdeuterated protein samples and that those corrections might differ slightly for our U-[^{13}C,^{15}N]-$^1H/^2H$ labeled protein samples.

2.3.4 Bioinformatics

All PBPs for which structural and functional data is available (Berntsson et al., 2010; Chu & Vogel, 2011) were used for a multiple sequence alignment with FepB (UniProt ID: P0AEL6) using ClustalW2 (http://www.ebi.ac.uk/Tools/clustalw2). The output from the alignment was subsequently used as input for the Phylip package (http://evolution.genetics.washington.edu/phylip.html). A distance matrix was created based on the Dayhoff PAM method and the phylogenetic tree was generated using the Fitch-Margoliash tree drawing method. A statistical estimate of the confidence of the branching in the tree was determined using the bootstrap method. The above-mentioned procedure was repeated for FepB with only the PBPs in cluster A.

2.4 Results and Discussion

A pairwise sequence alignment between FepB and the 120 PBPs for which structural and functional data is available (Berntsson et al., 2010; Chu & Vogel, 2011), indicates that the sequence identity is on average only $6.3 \pm 4.0\%$, with a maximum of 20%. Despite the fact that several homologous proteins are present in the data set, the average sequence identity for the complete pairwise alignment is only $6.9 \pm 5.6\%$ and confirms earlier findings that PBPs have vary diverse primary sequences. As noted earlier by Berntsson et al. (2010), the phylogenetic analysis based on the multiple sequence alignments is difficult due to the aforementioned low sequence identity. Nevertheless, from the analysis of all PBPs it was clear that the primary sequence of FepB clusters together with sequences of PBPs that are found in cluster A (data not shown). We, therefore, performed the bioinformatics analysis again but now with only sequences from cluster A. Figure 2.3 indicates that, based on the sequence alignments, FepB is more closely related to PBPs in cluster A-II (Berntsson et al., 2010). While the separation from subcluster I is apparent, one cannot make other conclusive statements based on the phylogenetic tree because the confidence on the branching points, determined using the bootstrap method, is rather low.

All proteins in cluster A possess an interdomain α-helix and the further division in subclusters I and II is consistent with conformational differences in this α-helix. Cluster A-I consists of proteins with a $\sim$20-residue α-helix (similar to FhuD), while a 2–3 residue 3_{10} helix is found at the start of the slightly longer α-helix ($\sim$25 residues) for proteins in subcluster II (Chu & Vogel, 2011).

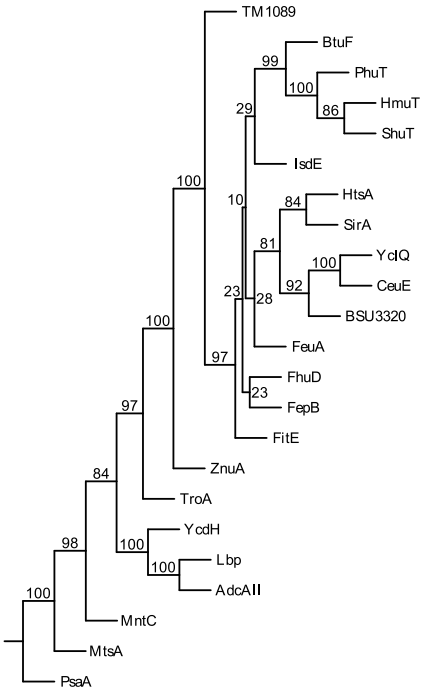

Figure 2.3. Phylogenetic tree for FepB and the structural characterized PBPs in cluster A based on multiple sequence alignment. The values at the branching points are determined by the bootstrap method and indicate the percentage that this branching consistently occurred.

2.4.1 NMR Spectroscopy and Resonance Assignments

Despite comprehensive efforts over the past years to obtain crystals for FepB, no suitable crystallization conditions were found for apo- or holo-FepB, thereby preventing structural studies of this PBP using X-ray crystallography (Krewulak, 2005). NMR spectroscopy circumvents the need for diffracting crystals, but its application to obtain a high-resolution structure for a 34 kDa, single-chain protein is not straightforward. The methodology to obtain NMR resonance assignments for backbone nuclei is, however, well established and involves a combination of advances in biochemical labeling methods (e.g., deuteration) and NMR methodology (e.g., TROSY) (see, for example, the review by Gardner & Kay (1998) and Wider & Wüthrich (1999)). The dilution of the highly polarized ^{1}H spins by deuteration greatly improves the sensitivity and spectral resolution of NMR spectra for high molecular weight systems, but the concomitant reduction in the number of available NOE-based distance restraints severely impedes the determination of a high-resolution structure (Gardner et al., 1997). Even though the determination of a high-resolution, three-dimensional structure of such large proteins remains a challenging task, information obtained from NMR data can give insight into protein function even in the absence of a structure.

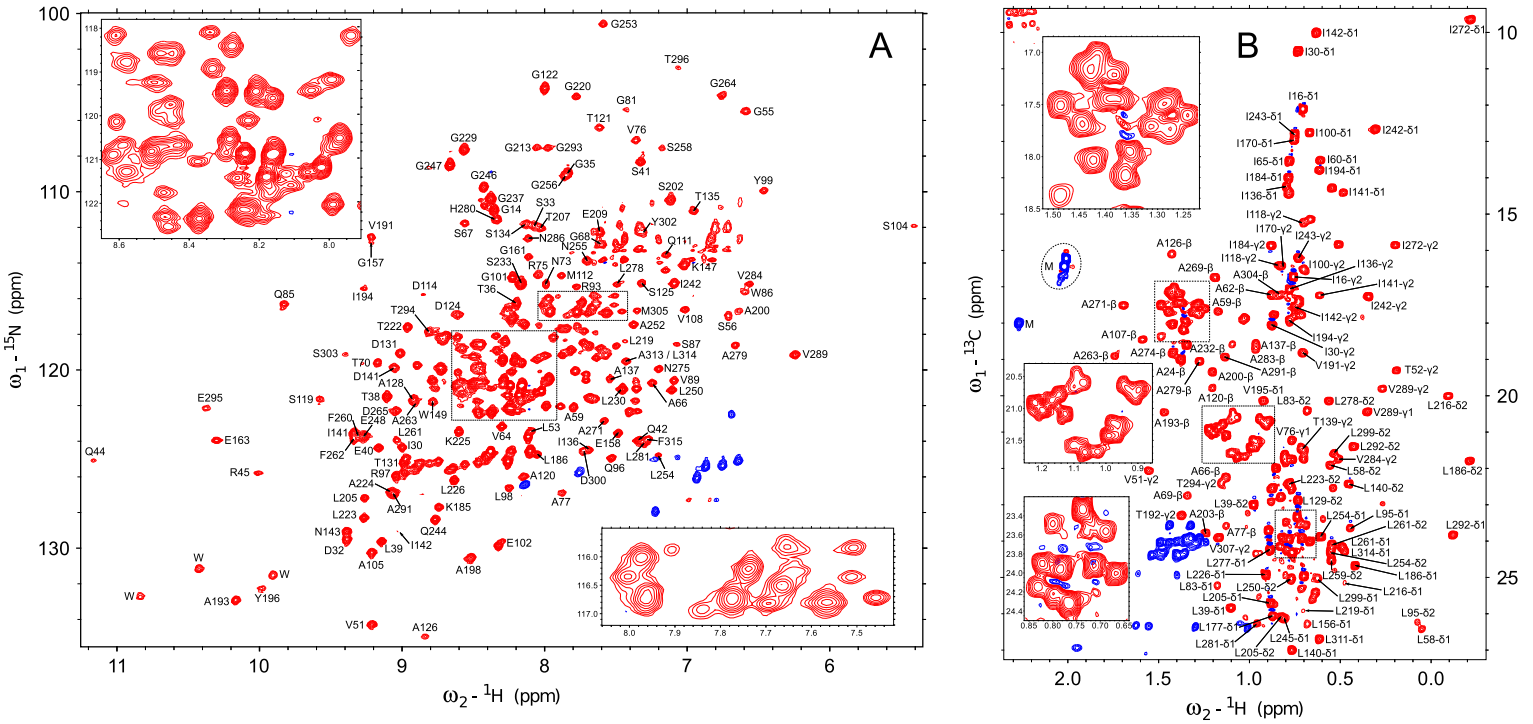

Figure 2.4. [^{1}H-^{15}N]-TROSY-HSQC (panel A) and the CHD_2-detected CT-[^{1}H-^{13}C]-HSQC (panel B) spectrum of apo-FepB recorded at 25 °C. (A) A subset of the peaks assigned to backbone residues are labeled by their one-letter amino acid code and residue number; negative (blue) signals originate from Arg side chain NH_2, and cross-peaks tentatively assigned to Trp side chain indole protons are designated by W. The weak signal pairs near 110–114 (^{15}N) and 6.6–7.5 (^{1}H) ppm originate from Gln/Asn side chain NH_2 and have not been assigned. (B) A subset of the cross-peaks of the stereospecifically assigned methyl groups are labeled by their one-letter amino acid code and residue number, negative (blue) signals between 1.2 and 1.5 ppm originate from CHD methylene groups and (unassigned) signals belonging to Met are designated by M.

Figure 2.4 illustrates the [^{1}H$-^{15}$N]-TROSY-HSQC (panel A) and the CHD_2-detected CT-[^{1}H$-^{13}$C]-HSQC (panel B) spectrum of the U-[^{13}C,^{15}N]-^{1}H/^{2}H apo-FepB sample, the same data for holo-FepB is shown in the Appendix (Figure A2.1). High-quality spectra with excellent sensitivity and resolution were obtained for both systems and thus provide a good starting point for an in-depth investigation using NMR spectroscopy.

Protein expression in a bacterial growth medium containing U-[^{1}H,^{13}C]-D-glucose as the sole carbon source and ~100% D_2O yields NMR samples that are highly deuterated at aliphatic carbon positions while all methyl groups are isotopically enriched with ^{1}H (*cf.* Figure 2.4, panel B) (Rosen et al., 1996; Shekhtman et al., 2002; Otten et al., 2010). In particular, $^{13}C^{\alpha}$ positions are >95% deuterated and high deuterium incorporation levels are found for $^{13}C^{\beta}$ positions as well, with the exception of Ser, Cys, and Trp residues (Rosen et al., 1996; Otten et al., 2010). Of note, since all NMR measurements for obtaining the backbone assignment are "out-and-back" $^{1}H^{N}$-detected experiments it is of great importance that a (nearly) complete back-exchange of amide protons is achieved after the bacterial expression. In the case of FepB, as in most other studies, it is assumed that during the protein purification in H_2O the deuterium nuclei at all labile positions are exchanged by protons. In some cases (e.g., malate synthase G (Tugarinov et al., 2002)) an additional unfolding/refolding step is, however, necessary to accomplish this goal.

The combination of deuteration and TROSY-variants of the standard NMR experiments yielded a nearly complete assignment of the $^{1}H^{N}$, ^{15}N, $^{13}C'$, $^{13}C^{\alpha}$, and $^{13}C^{\beta}$ chemical shifts for both apo-FepB (95%) and holo-FepB (96%). Significant residual protonation on $^{13}C^{\beta}$ positions was only observed for Ser residues, but did not hamper the assignment procedure. A closer inspection of the [^{1}H$-^{15}$N]-TROSY-HSQC spectrum (Figure 2.4, panel A), shows that not all cross-peaks exhibit uniform line widths and intensities. Interestingly, most residues for which the assignments are incomplete or absent (residues 46–47, 57–60, 115–118, 140–142, and 159–160) could neither be observed in the apo- nor the holo-state of the protein. The fact that these correlations are absent/weak in both states of the protein makes it unlikely to be an effect of ligand binding. The observation might be caused by the aforementioned (incomplete) back-exchange, but is in other studies also attributed to exchange processes on the intermediate time scale (e.g., conformational exchange and/or fast proton exchange with the solvent). While incomplete back-exchange cannot be excluded as a reason for the missing/weak signals in the [^{1}H$-^{15}$N]-TROSY-HSQC spectrum, the titration of apo-FepB with

gallium enterobactin toward the holo-state of the system (data not shown) supports the hypothesis of a conformational equilibrium between the different possible states (see Figure 2.2). Considering the high binding affinity of enterobactin (in the nM range), the addition of substoichiometric amounts is expected to result in a superposition of the spectra for the apo- and holo-states (slow exchange regime). In stark contrast to this prediction, however, several resonances weaken or disappear completely in the course of the titration and these effects correlate with the chemical shift differences between the two end states, suggesting that it is due to conformational exchange. Moreover, similar effects are observed for side chain methyl groups and for these resonances it can be excluded that incomplete back-exchange or fast proton exchange with the solvent is the origin. In conclusion, our NMR data show indications of an equilibrium between different states of the protein, but further experiments are needed to fully characterize this dynamical process.

In addition, our biochemical labeling scheme yields $^{13}CHD_2$ methyl groups with high abundance for all methyl-containing amino acids and these can be sequence-specifically assigned to near completion, using ^{13}C TOCSY NMR spectroscopy (Otten et al., 2010). In the case of FepB, a nearly complete assignment of the methyl groups was obtained (85% and 76% for apo-FepB and holo-FepB, respectively). It is worth noting that these percentages are lower limits in the sense that more methyl resonances are present in the 3D C-TOCSY-CHD_2 experiment, but since signals for these methyl-containing amino acids are not present in the backbone experiments (see above) they cannot be sequence-specifically assigned. The backbone and methyl group assignments of apo- and holo-FepB are given in the Appendix (Tables A2.3 and A2.4, respectively).

2.4.2 Secondary Structure of Apo- and Holo-FepB

The obtained backbone chemical shift assignments can be used to identify secondary structure elements in FepB by calculating the difference between the observed chemical shifts and their corresponding "random-coil value". After the introduction of this concept in the early 90's by the groups of Jardetzky, Suadek, Richards and others (Szilágyi & Jardetzky, 1989; Pastore & Saudek, 1990; Wishart et al., 1992; Wishart & Sykes, 1994), several alternative definitions of the "random-coil values" have been reported, for example by including corrections for sequence effects (Schwarzinger et al., 2001; Wang & Jardetzky, 2002). In the current study,

we have used the **n**eighbor **c**orrected **S**tructural **P**ropensity **C**alculator (ncSPC) for which the random-coil database and the neighbor corrections are based solely on BioMagResBank (Ulrich et al., 2008) entries of intrinsically disordered proteins (Tamiola et al., 2010). All chemical shifts ($^{1}H^{N}$, ^{15}N, $^{13}C'$, $^{13}C^{\alpha}$, and $^{13}C^{\beta}$) were used to calculate the secondary structure propensity for apo- and holo-FepB (see the Appendix, Figure A2.2 for scores per nucleus) and the combined, consensus score is shown in Figure 2.5 (panels A and B, respectively). Positive values in this consensus ncSP score are indicative of α-helical content, while negative scores reveal β-strands. The consensus secondary structure elements for apo-FepB are shown in panel C (Figure 2.5), while the difference between the $ncSP_{holo}$ and $ncSP_{apo}$ score is presented in panel D.

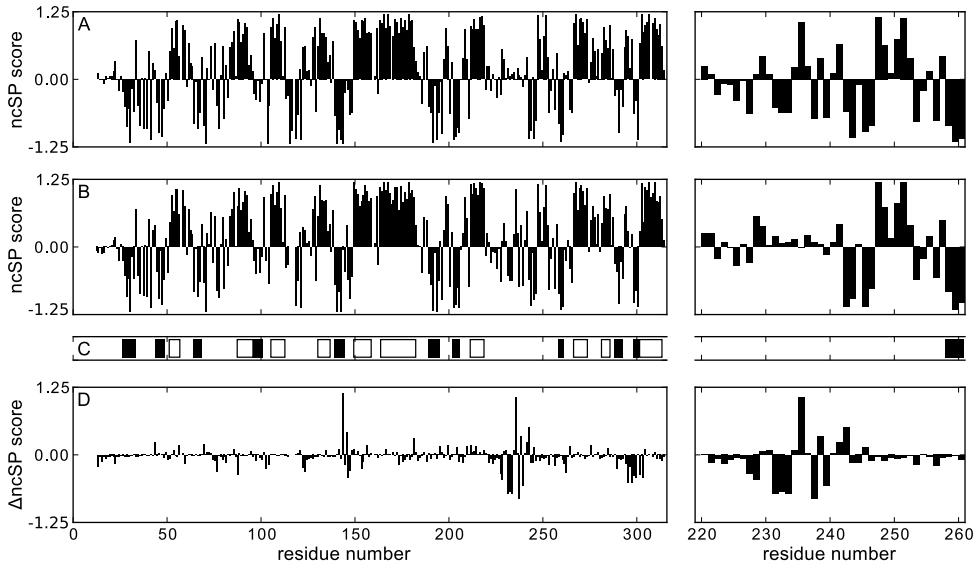

Figure 2.5. Consensus ncSP score for apo- and holo-FepB (panels A and B), overall topology of FepB (panel C; □ helix, ■ beta), and the difference ($ncSP_{holo}$ − $ncSP_{apo}$) between the two states (panel D).

From Figure 2.5 it is apparent that the overall topology of FepB is mixed α/β, and consists of approximately 10 helical and sheet regions. The observed secondary structure elements of FepB are in good agreement with the global fold of other PBPs from cluster A, which are all comprised of two globular, mixed α/β-domains (Rossmann-fold) and an interdomain α-helix. These findings confirm the prediction from the bioinformatics analysis that FepB is part of this specific cluster of PBPs. The binding of gallium enterobactin does not really affect the overall topology of

the protein, even though in a few regions (residues 143–147, 227–242, and 294–302) significant deviations are observed (see Figure 2.5, panel D). A positive/negative value for the difference in ncSP score between the two states indicates that such region became less/more extended upon ligand binding. Ligand binding is accompanied with a transition from coil to beta for residues 227–242 and from alpha to more extended for the latter region.

2.4.3 Ligand-Induced Chemical Shift Changes

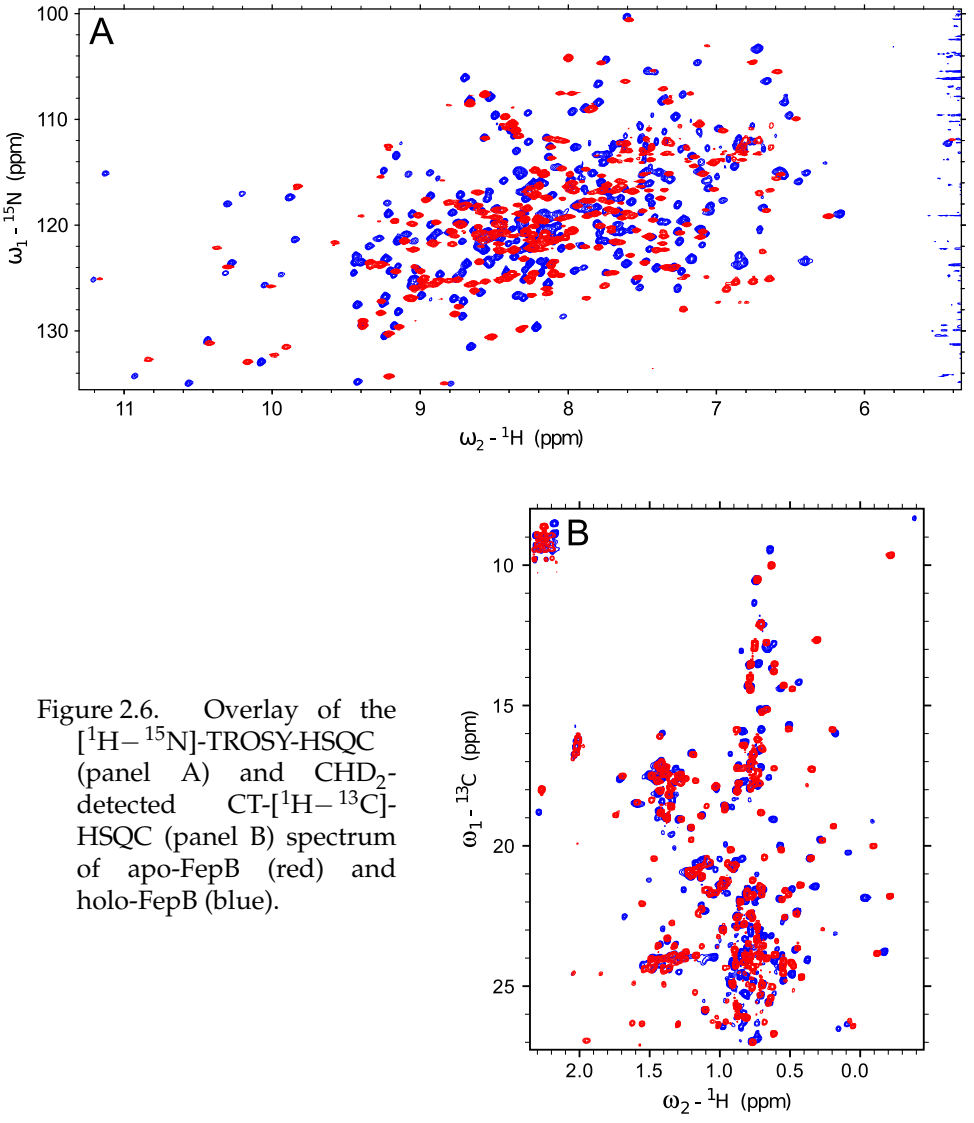

Figure 2.6. Overlay of the [^{1}H−^{15}N]-TROSY-HSQC (panel A) and CHD_2-detected CT-[^{1}H−^{13}C]-HSQC (panel B) spectrum of apo-FepB (red) and holo-FepB (blue).

Substantial chemical shift perturbations upon ligand binding can be observed in Figure 2.6, both for backbone amide as well as for side chain methyl group resonances. All backbone and side chain resonances for which assignments are available in both apo- and holo-FepB have been used to probe for structural changes due to binding of gallium enterobactin. All nuclei show significant chemical shift changes (see the Appendix, Figure A2.3), with maximum absolute differences of 1.2, 6.8, 3.5, 2.6, 2.4, 0.28, and 1.1 ppm for $^{1}H^{N}$, ^{15}N, $^{13}C'$, $^{13}C^{\alpha}$, $^{13}C^{\beta}$, $^{1}H^{M}$, and $^{13}C^{M}$, respectively.

The combined chemical shift perturbation for backbone nuclei and side chain methyl groups is calculated as described in "Materials and Methods" and the results are shown in Figure 2.7 (panels A and B, respectively). It is worth noting that chemical shift changes are consistently observed for all different probes and, moreover, throughout most of the primary sequence of the protein, except for the first 50 N-terminal residues. Carbon chemical shifts, and in particular $^{13}C^{\alpha}$ and $^{13}C^{\beta}$, are highly sensitive to ϕ/ψ torsion angles and, therefore, the regions showing large chemical shift perturbation for those nuclei correlate with the observed changes in structural propensity (*cf.* Figures 2.5 and A2.3). Amide protons and side chain methyl groups, on the other hand, are strong reporters of local tertiary structure (e.g., proximity to aromatic residues, hydrogen bonds, and hydrophobic effects) (Mulder & Filatov, 2010) and complement the information obtained from $^{13}C/^{15}N$ backbone chemical shifts. Unifying the aforementioned results suggest that the overall topology upon ligand binding is hardly altered, and that the observed chemical shift differences report mainly on local changes in the hydrophobic interior of the protein and/or rearrangements in the domain interface.

For comparison we show in Figure 2.7 also the backbone chemical shift mapping for maltose binding protein (MBP) upon binding to maltotriose and β-cyclodextrin (panels C and D, respectively), calculated using the chemical shift assignments from Kay and co-workers (BMRB entries: 4354, 4987, and 4987) (Gardner et al., 1998; Evenäs et al., 2001). MBP is a periplasmic binding protein that belongs to cluster B and has been extensively studied both by X-ray crystallography and NMR spectroscopy (Sharff et al., 1992, 1993; Quiocho et al., 1997; Gardner et al., 1998; Evenäs et al., 2001). High-resolution X-ray structures are available for the apo form of the protein as well as for different ligand-bound states. These studies have established that MBP adopts an open conformation in the absence of the ligand and that large conformational changes ($\sim$35° domain closure, "Venus flytrap"-type motion) take place upon binding of the ligand, while retaining the same

overall topology. Residual dipolar coupling (RDC) data confirmed the domain reorientation upon binding of maltotriose, but also revealed significantly more domain closure ($\sim$14°) in the case of β-cyclodextrin than deduced from the crystal structures ($\sim$2°). In the case of MBP the chemical shift perturbations, although observed throughout the primary sequence, are limited to the ligand binding site and the domain interface in its immediate surrounding. Of note, the chemical shift perturbations upon binding of maltotriose or β-cyclodextrin are confined to the same regions of the protein, but the magnitude is on average two to three times smaller in the latter case (*cf.* Figure 2.7, panels C and D) in qualitative agreement with the difference in closure angle (Evenäs et al., 2001). It is important to realize, however, that from this NMR data alone it is not possible to determine if the closure angle of $\sim$14° is a static value or, alternatively, represents an "average" reflecting the proposed dynamic equilibrium between the different possible states of the protein (see Figure 2.2).

It is difficult to interpret the chemical shift perturbation data in a quantitative manner because there is no high-resolution structure of FepB available. However, it is fair to conclude that from the comparison of the data obtained for FepB and MBP, a "Venus flytrap"-type of binding mode seems to be a plausible possibility for FepB.

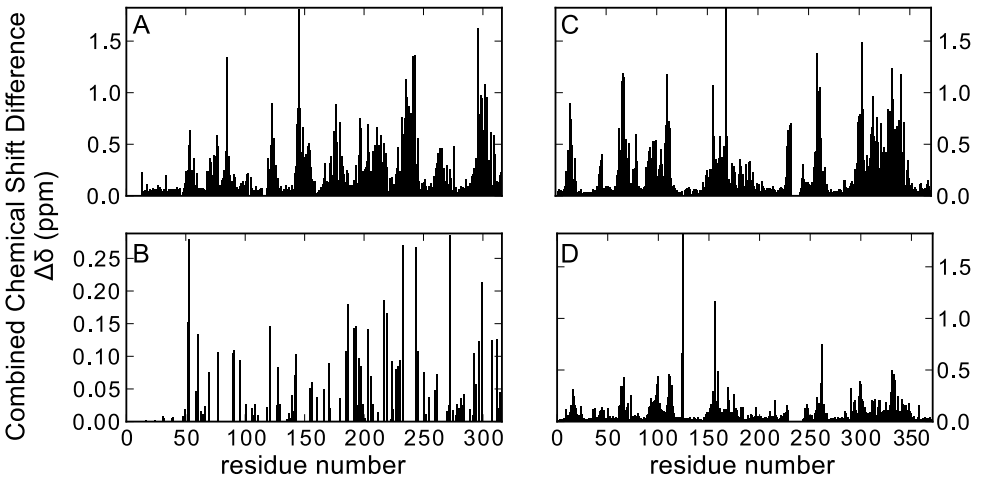

Figure 2.7. Combined chemical shift differences between apo- and holo-FepB for backbone (panel A) and methyl groups (panel B). Consensus backbone chemical shift mapping for maltose binding protein upon binding to maltotriose (panel C, max: 2.1 ppm) and β-cyclodextrin (panel D, max: 2.6 ppm).

2.4.4 Protein Dynamics

Backbone ^{15}N relaxation measurements were performed on apo- and holo-FepB to examine if the fast (ps–ns) time scale backbone dynamics are influenced by the binding of the ligand.

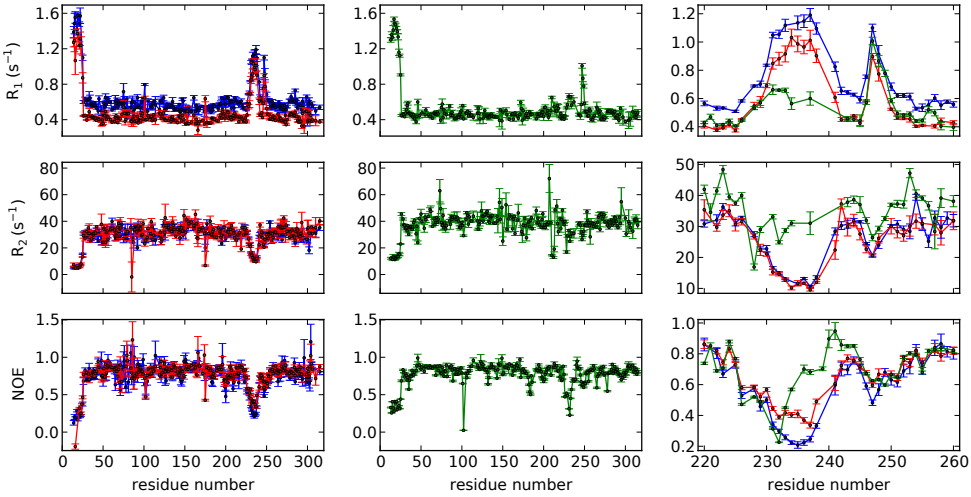

Figure 2.8. ^{15}N relaxation parameters of apo-FepB recorded at 600 (red) and 800 (blue) MHz (left panel), holo-FepB recorded at 700 MHz (middle panel), and a more detailed comparison of the loop dynamics (residues 225–250) upon ligand binding (right panel).

The data for apo-FepB recorded at 600 and 800 MHz and the data for holo-FepB recorded at 700 MHz are shown in Figure 2.8 (left and middle panels, respectively). It is important to note that the absolute values of R_1, R_2 and $\{^1\text{H}\}$-^{15}N NOE cannot be compared directly because the data was recorded at different magnetic field strengths. A qualitative interpretation is, however, possible and this will be discussed below. The data in the left panel (Figure 2.8) indicates that overall apo-FepB is well ordered (high NOE values and uniform values for R_1 and R_2), with the exception of the first 25 N-terminal residues of the protein and a flexible region between residues 225 and 250. Upon ligand binding (Figure 2.8, middle panel) the N-terminal part of the protein remains highly flexible, while the dynamics of the mobile loop is largely suppressed. In the right panel (Figure 2.8) an inset is shown for this part of the protein which demonstrates that the flexibility in the first part of the loop (residues 225–232) is similar, but that the remainder has become more rigid upon ligand binding. Holo-FepB seems to exhibit slightly more dynamic around residues 102 and 183, but the differences are not as large as for the above-mentioned extended loop.

The predicted protein flexibility based on chemical shift data as described by Berjanskii & Wishart (2005) is in good agreement with the information obtained from the measured ^{15}N relaxation parameters. Their algorithm calculates the flexibility from a "Random Coil Index" (RCI) by comparing the experimental data and expected random coil values, and shows reasonable correlation with the Modelfree order parameter (S^2) derived from NMR relaxation measurements.

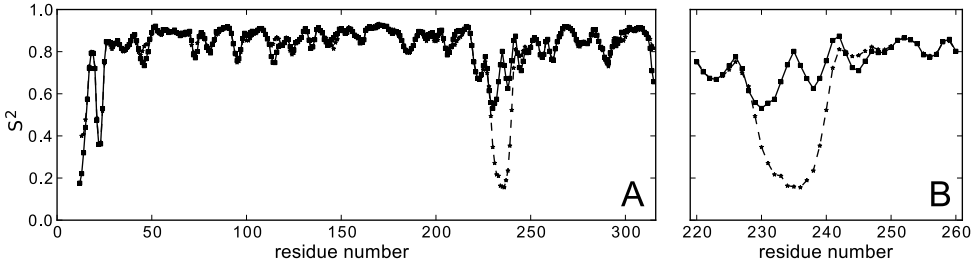

Figure 2.9. Predicted order parameter for apo- (--★--) and holo-FepB (-■-) based on the chemical shift data.

In Figure 2.9 the result of the RCI prediction is shown for apo- and holo-FepB based on the assigned $^{1}H^{N}$, ^{15}N, $^{13}C'$, $^{13}C^{\alpha}$, and $^{13}C^{\beta}$ chemical shifts. The predicted S^2 is highly uniform and similar for both systems, showing only increased flexibility for the first ~25 residues and the region between residues 225 and 250. Moreover, the predicted behavior of the loop region and the measured effect upon ligand binding are identical: the first part of the loop remains flexible while the latter part becomes more rigid when the ligand is bound.

2.4.5 Ligand Binding and Comparison with Data for Other PBPs

Previously obtained results of a sequence alignment of FepB with its homologues from other organisms show that there are several conserved residues (e.g., Phe, Tyr, Glu/Asp, Arg, and Trp) which are, based on homology modeling with FhuD, implicated in the formation of the ligand binding site or represent solvent-exposed residues that might interact with the inner membrane transporter (Krewulak, 2005). From fluorescence results it is clear that (some) Trp residues respond to the addition of ferric enterobactin and are, therefore, involved in the formation of the ligand binding site or at least in close proximity. Of note, there is a decrease in quantum yield rather than a shift in the emission maximum, indicating that the environment of the Trp residues does not really change upon ligand binding (Krewulak, 2005).

As described earlier, the conformational change upon ligand binding varies significantly between PBPs from the different structural clusters. For PBPs in cluster A, in particular, there are conflicting observations from both experimental and computational approaches. For some systems (e.g., FitE, FeuA, and HmuT) large, hinged motions are observed (*cf.* PBPs in clusters B–F), while others (e.g., FhuD, FhuD1, and FhuD2) show only modest interdomain motion. Finally, there are even PBPs (e.g., BtuF, ShuT, PhuT, ZnuA, and TroA) for which ligand binding does not seem to significantly alter the overall structure. In the case of ZnuA and TroA, both proteins belonging to subcluster A–I (Berntsson et al., 2010), there is a hinge-like motion of a few degrees, and the binding of the Zn^{2+} ion is mainly accompanied by changes in some loops (Lee et al., 1999, 2002; Yatsunyk et al., 2008). More recently, the structures of the apo- and holo-forms of HtsA (Beasley et al., 2009; Grigg et al., 2010b) and SirA (Grigg et al., 2010a) have been solved by X-ray crystallography. Both proteins are member of cluster A–II and bind the siderophores staphyloferrin A and B, respectively. The conformational changes upon ligand binding are similar to those observed for ZnuA and TroA, namely little hinge motion between the domains, but (large) localized conformational changes in the loops that form part of the binding site. A possible explanation for the difference in ligand binding modes could be the actual size of the ligand, as was pointed out by Lee and coworkers (Lee et al., 1999). PBPs can bind a wide variety of ligands with different sizes and these range from ions (e.g., Zn^{2+}, 1.5 Å^3; SO_4^{2-}, 66.5 Å^3) to maltodextrin (882.3 Å^3). The commonly accepted "Venus flytrap" binding mode implies that two requirements are met: (i) the bending motion is wide enough to accommodate the exchange of the ligand between the binding site and solvent, and (ii) the closed form is significantly stabilized upon ligand binding (i.e., sum of the energy gained by ligand binding and lost to changes of entropy is sufficiently high). In other words, for small ligands the required hinge motion for binding is only modest and high-affinity binding can only be achieved by an almost pre-formed binding site, because otherwise the entropic costs would be too high. For bigger ligands (e.g., enterobactin, $\sim$545 Å^3), a larger hinge bending is expected to allow for the actual ligand binding/release. The binding of such ligands can be associated with a larger entropic penalty (e.g., ordering of a mobile hinge region), because the change in free energy upon binding is bigger than for small ions.

For other catecholate-type siderophore binding PBPs (e.g., CeuE, YclQ, and FeuA), it has been observed that basic amino acids (Arg/Lys) are present in the active site, presumably to accommodate the negatively charged ferric-siderophore ligand. Unexpectedly, these conserved residues are not present in FepB, which could point

to a different binding mode for this specific PBP. However, from the NMR data presented here, we cannot draw definite conclusions on the binding mode of FepB. It is clear that the loop dynamics is altered upon ligand binding (see Figure 2.8), which might point to a similar binding mode as observed for SirA (Grigg et al., 2010a) and HtsA (Beasley et al., 2009; Grigg et al., 2010b), both found in the Gram-positive *Staphylococcus aureus*. On the other hand, the chemical shift perturbation data and comparison to MBP (see Figure 2.7), indicates that a "Venus flytrap" type of binding is a possible scenario as well. It is tempting to speculate on the difference between PBPs from Gram-positive and Gram-negative bacteria (the former showing the "Venus flytrap" most prominently), but relying only on X-ray structures remains a delicate issue here. As has been demonstrated in the case of β-cyclodextrin/MBP, the opening angle is significantly affected by crystal packing effects (Evenäs et al., 2001), and, therefore, one needs to be cautious in using only static structures to deduce the binding mode. Additional structural information of (more) PBPs is needed before general conclusions can be drawn, and solution state NMR is able to provide such information, either by solving the solution structures of the apo- and holo-state or by providing information on the relative domain orientations (e.g., using RDC data). Research along these lines on the different structural states of FepB is currently pursued in our laboratories.

2.5 Acknowledgment

We thank Dr. Lewis Kay for sharing with us some of the Varian NMR pulse sequence codes used in this study and Prof. Bert Poolman for his continuous support. Dr. Ronnie P.-A. Berntsson is acknowledged for sharing the data used for the classification of the PBPs and we are grateful to Prof. Geerten Vuister and Dr. Marco Tessari (Radboud University Nijmegen) for providing measurement time on the 800 MHz spectrometer and their help in setting up the relaxation experiments. This work was supported by a VIDI grant to F.A.A.M. from The Netherlands Organization for Scientific Research (NWO) and a grant to H.J.V. from the Canadian Institutes for Health Research. H.J.V. holds a Scientist award from the Alberta Heritage Foundation for Medical Research.

2.6 Appendix

Table A2.1. Experimental Details for the NMR Experiments Performed To Obtain the Assignments of FepB[a]

Experiments on apo-FepB	Number of complex points				Max. evolution time (ms)				d_1 (s)	nt	exp. time (hours)	Reference
	n_1	n_2	n_3	n_4	t_1	t_2	t_3	t_4				
2D TROSY-[^{1}H$-^{15}$N]-HSQC[b]	128 (N)	640 (H)	-	-	51.2	64.0	-	-	1	4	2	Weigelt (1998)
3D TROSY-HNCO[c]	80 (C)	24 (N)	768 (H)	-	37.9	13.3	76.8	-	1.4	8	28	Salzmann et al. (1998)
3D TROSY-HN(CA)CO[c]	62 (C)	24 (N)	768 (H)	-	29.3	13.3	76.8	-	1.4	32	72	Salzmann et al. (1999)
3D TROSY-CT-HNCA[b]	88 (C)	43 (N)	576 (H)	-	23.2	21.5	64.0	-	1.1	16	86	Yang & Kay (1999b)
3D TROSY-CT-HN(CO)CA[b]	88 (C)	38 (N)	576 (H)	-	23.2	19.0	64.0	-	1.3	16	88	Yang & Kay (1999b)
3D TROSY-HN(COCA)CB[b]	50 (C)	32 (N)	576 (H)	-	6.9	16.0	64.0	-	1.3	32	86	Yang & Kay (1999b)
3D TROSY-HN(CA)CB[b]	50 (C)	42 (N)	576 (H)	-	6.9	21.0	64.0	-	1.3	32	111	Yang & Kay (1999b)
4D TROSY-HNCO$_{i-1}$CA$_i$[b]	18 (C′)	18 (C$^{\alpha}$)	34 (N)	576 (H)	9.9	6.1	17.0	64.0	1.2	4	132	Konrat et al. (1999)
3D ^{15}N-NOESY-HSQC[b]	200 (H)	48 (N)	576 (H)	-	22.2	18.3	64.0	-	1.3	4	63	Marion et al. (1989)
2D CHD$_2$-detected [^{1}H$-^{13}$C]-HSQC[b]	111 (C)	512 (H)	-	-	27.8	64.0	-	-	1	32	2	Otten et al. (2010)
3D C-TOCSY-CHD$_2$[b]	75 (C)	111 (C^M)	512 (H)	-	6.3	27.75	64.0	-	3	2	58	Otten et al. (2010)

Experiments on holo-FepB	Number of complex points				Max. evolution time (ms)				d_1 (s)	nt	exp. time (hours)	Reference
	n_1	n_2	n_3	n_4	t_1	t_2	t_3	t_4				
2D TROSY-[^{1}H$-^{15}$N]-HSQC[c]	128 (N)	1024 (H)	-	-	45.9	81.1	-	-	1.3	128	13	Czisch & Boelens (1998)
3D TROSY-HNCO[c]	31 (C)	20 (N)	768 (H)	-	14.7	9.6	76.8	-	1	8	9	Salzmann et al. (1998)
3D TROSY-HN(CA)CO[c]	31 (C)	20 (N)	768 (H)	-	14.7	9.6	76.8	-	1	32	27	Salzmann et al. (1999)
3D TROSY-HNCA[c]	90 (C)	50 (N)	768 (H)	-	14.6	17.9	76.8	-	1	8	49	Eletsky et al. (2001)
3D TROSY-HN(CO)CA[c]	32 (C)	20 (N)	768 (H)	-	6.1	9.6	76.8	-	1.3	8	9	Salzmann et al. (1999)
3D TROSY-HN(CO)CACB[c]	64 (C)	20 (N)	768 (H)	-	6.1	9.6	76.8	-	1	32	57	Salzmann et al. (1999)
3D TROSY-HNCACB[c]	63 (C)	20 (N)	768 (H)	-	6.1	9.6	76.8	-	1	32	56	Salzmann et al. (1999)
3D TROSY-^{15}N-NOESY-HSQC[c]	64 (H)	24 (N)	1024 (H)	-	6.6	8.6	104.9	-	1	32	80	Zhu et al. (1999)
2D CHD$_2$-detected [^{1}H$-^{13}$C]-HSQC[b]	111 (C)	512 (H)	-	-	27.8	64.0	-	-	1	32	2	Otten et al. (2010)
3D C-TOCSY-CHD$_2$[b]	75 (C)	111 (C^M)	512 (H)	-	6.3	27.75	64.0	-	3	2	58	Otten et al. (2010)

[a] Data recorded at 25 °C. [b] Data recorded on a Varian Inova 600 MHZ spectrometer. [c] Data recorded on a Bruker Avance 700 MHZ spectrometer.

Table A2.2. Experimental Details for the ^{15}N Backbone Relaxation NMR Experiments on FepB[a]

Experiments on apo-FepB[b]	Number of complex points		Max. evolution time (ms)		d_1 (s)	nt	exp. time (hours)	Reference
	n_1	n_2	t_1	t_2				
TROSY-[^{15}N]-T_1	128 (N)	512 (H)	51.2	56.9	3	8	38.5[d]	Farrow et al. (1994)
	128 (N)	626 (H)	36.6	56.9	3	8	34[d]	Farrow et al. (1994)
TROSY-[^{15}N]-$T_{1\rho}$	128 (N)	512 (H)	51.2	56.9	3	8	27[d]	Akke & Palmer (1996)
	128 (N)	626 (H)	36.6	56.9	3	8	27[d]	Akke & Palmer (1996)
TROSY-{^{1}H}-^{15}N NOE	128 (N)	512 (H)	49.2	64.0	10	8	81[d]	Farrow et al. (1994)
	128 (N)	704 (H)	36.6	64.0	11	8	101[d]	Farrow et al. (1994)

Experiments on holo-FepB[c]	Number of complex points		Max. evolution time (ms)		d_1 (s)	nt	exp. time (hours)	Reference
	n_1	n_2	t_1	t_2				
TROSY-[^{15}N]-T_1	128 (N)	1024 (H)	45.9	104.9	1	8	9[d]	Zhu et al. (2000)
TROSY-[^{15}N]-T_2	128 (N)	1024 (H)	45.9	104.9	1	16	18[d]	Zhu et al. (2000)
TROSY-{^{1}H}-^{15}N NOE	128 (N)	1024 (H)	46.2	91.8	5	32	47[d]	Zhu et al. (2000)

[a] Data recorded at 25 °C. [b] Data recorded at 600 (first row) and 800 (second row) MHz. [c] Data recorded at 700 MHz. [d] Total experimental time for the complete measurement series.

Table A2.3. Backbone and Side Chain Assignments of Apo-FepB

Residue	^{1}H^N	^{15}N	^{13}C′	^{13}C$^\alpha$	^{13}C$^\beta$
S13	-	-	175.1	58.40	62.91
G14	8.357	111.0	173.8	44.81	
H15	8.165	119.6	174.7	55.37	29.11
I16	8.115	123.8	175.8	60.83	37.91
I16	C$^{\gamma 1}$: 26.10	C$^{\delta 1}$: 12.11	H$^{\delta 1}$: 0.709	C$^{\gamma 2}$: 16.75	H$^{\gamma 2}$: 0.760
D17	8.370	124.4	176.1	54.22	40.60
D18	8.177	121.3	176.3		
D19	8.238	120.9	176.4	54.38	40.50
D20	8.159	120.9	176.6	54.21	40.27
K21	8.023	121.2	176.8	55.96	31.50
H22	8.297	119.4	174.9	55.40	28.20
M23	8.262	122.1	175.8	55.21	32.08
M23[b]	C$^{\epsilon}$: -	H$^{\epsilon}$: -			
A24	8.260	125.1	177.3	51.75	18.81
A24[c]	C$^{\beta}$: 19.00	H$^{\beta}$: 1.380			
D25	8.275	120.6	174.4	54.68	40.63
W26	7.788	120.1	174.2	54.78	30.38
P27			175.9	62.11	36.15
R28	8.686	118.0	173.7	54.47	32.32
Q29	8.506	120.8	175.5	54.09	29.73
I30	9.002	124.3	175.7	57.76	39.38
I30	C$^{\gamma 1}$: 26.01	C$^{\delta 1}$: 10.57	H$^{\delta 1}$: 0.734	C$^{\gamma 2}$: 18.10	H$^{\gamma 2}$: 0.880
T31	8.989	125.2	174.4	61.52	69.83
T31	C$^{\gamma 2}$: 21.09	H$^{\gamma 2}$: 1.131			
D32	9.389	129.5	177.4	52.08	42.24
S33	8.075	111.9	175.6	60.37	62.72
R34	8.433	120.6	176.1	54.33	29.74
G35	7.837	108.9	171.2	44.28	
T36	8.192	116.3	173.8	62.04	69.19
T36	C$^{\gamma 2}$: 21.43	H$^{\gamma 2}$: 0.997			
H37	8.986	125.8	174.0	53.51	30.31
T38	9.101	121.5	174.2	62.56	69.27
T38	C$^{\gamma 2}$: 21.67	H$^{\gamma 2}$: 1.070			
L39	9.145	129.6	176.9	53.37	41.90
L39	C$^{\gamma}$: 26.85	C$^{\delta 1}$: 25.84	H$^{\delta 1}$: 1.103	C$^{\delta 2}$: 23.02	H$^{\delta 2}$: 0.979
E40	9.164	124.3	175.6	58.73	29.74
S41	7.326	108.3	171.7	55.72	64.71
Q42	7.339	123.9	174.6	53.04	27.50
P43			176.3	63.39	31.40
Q44	11.160	125.1	175.4	55.09	31.69
R45	10.010	125.7	174.6	54.62	31.96
I46[a]	-	-	-	-	-
V47	-	-	174.7	60.18	32.94
V47	C$^{\gamma 1}$: 22.78	H$^{\gamma 1}$: 0.828	C$^{\gamma 2}$: 22.55	H$^{\gamma 2}$: 0.876	
S48	7.852	118.3	175.5	55.15	64.04
T49	8.283	116.8	171.5	61.78	68.50
T49	C$^{\gamma 2}$: 20.61	H$^{\gamma 2}$: 1.073			
S50	7.627	116.2	174.6	54.09	63.29
V51	9.218	134.3	175.1	64.79	30.63
V51	C$^{\gamma 1}$: 18.61	H$^{\gamma 1}$: 1.098	C$^{\gamma 2}$: 22.08	H$^{\gamma 2}$: 1.557	
T52	7.841	117.0	179.7	66.76	68.32
T52	C$^{\gamma 2}$: 19.32	H$^{\gamma 2}$: 0.190			
L53	8.092	123.4	178.7	56.84	41.35
L53[a]	C$^{\gamma}$: -	C$^{\delta 1}$: -	H$^{\delta 1}$: -	C$^{\delta 2}$: -	H$^{\delta 2}$: -
T54	8.039	117.5	174.9	66.44	
T54	C$^{\gamma 2}$: 21.43	H$^{\gamma 2}$: 1.141			
G55	6.591	105.5	175.6	46.48	
S56	6.709	117.0	175.6	62.85	64.35
L57[a]	-	-	-	-	-
L58	-	-	181.2	56.86	39.55
L58	C$^{\gamma}$: 25.08	C$^{\delta 1}$: 26.41	H$^{\delta 1}$: 0.044	C$^{\delta 2}$: 21.91	H$^{\delta 2}$: 0.555
A59	7.797	122.1	178.5	54.86	17.59
A59[c]	C$^{\beta}$: 17.68	H$^{\beta}$: 1.174			
I60	-	-	172.7	59.62	36.64
I60	C$^{\gamma 1}$: 23.16	C$^{\delta 1}$: 13.55	H$^{\delta 1}$: 0.610	C$^{\gamma 2}$: 17.42	H$^{\gamma 2}$: 0.731
D61	7.736	116.2	174.8	55.30	38.22
A62	7.820	118.9	176.8	49.36	17.13
A62[c]	C$^{\beta}$: 17.26	H$^{\beta}$: 0.880			
P63			173.6	62.56	26.53
V64	8.299	123.1	174.8	57.58	32.10
V64	C$^{\gamma 1}$: 17.84	H$^{\gamma 1}$: 0.755	C$^{\gamma 2}$: 21.57	H$^{\gamma 2}$: 0.704	
I65	8.589	122.0	177.1	60.24	38.20
I65	C$^{\gamma 1}$: 25.34	C$^{\delta 1}$: 13.55	H$^{\delta 1}$: 0.780	C$^{\gamma 2}$: 17.80	H$^{\gamma 2}$: 0.869
A66	7.246	120.7	175.1	50.62	22.09
A66[c]	C$^{\beta}$: 22.25	H$^{\beta}$: 1.135			
S67	8.561	111.7	176.5	54.68	64.59
G68	7.604	112.9	171.0	45.80	
A69	7.402	122.3	177.9	50.61	22.58
A69[c]	C$^{\beta}$: 22.68	H$^{\beta}$: 1.338			
T70	9.171	119.6	171.4	57.52	70.07
T70	C$^{\gamma 2}$: 17.89	H$^{\gamma 2}$: 1.027			
T71	7.663	116.5	172.5	61.05	69.65
T71	C$^{\gamma 2}$: 20.90	H$^{\gamma 2}$: 1.159			
P72			177.1	62.70	31.83

Residue	$^{1}H^{N}$	^{15}N	$^{13}C'$	$^{13}C^{\alpha}$	$^{13}C^{\beta}$
N73	7.990	115.2	174.6	54.02	36.31
N74	-	-	175.8	50.26	37.36
R75	8.048	114.6	177.4	59.25	30.00
V76	7.356	107.1	176.0	60.27	32.39
V76	$C^{\gamma 1}$: 21.24	$H^{\gamma 1}$: 0.772	$C^{\gamma 2}$: 17.49	$H^{\gamma 2}$: 0.730	
A77	7.873	126.9	176.5	50.71	23.39
A77[c]	C^{β}: 23.59	H^{β}: 1.129			
D78	8.607	120.1	178.1	51.42	40.65
D79	8.258	116.6	176.4	55.48	39.39
Q80	8.160	117.2	175.7	54.28	29.87
G81	7.419	105.3	174.2	44.96	
F82	8.154	121.7	175.3	51.98	36.72
L83	-	-	178.4	54.93	37.22
L83	C^{γ}: 25.15	$C^{\delta 1}$: 25.22	$H^{\delta 1}$: 1.173	$C^{\delta 2}$: 20.50	$H^{\delta 2}$: 0.683
R84	7.746	119.0	178.3	60.00	30.42
Q85	9.838	116.4	174.7	57.51	25.17
W86	6.600	115.6	175.9	54.77	26.76
S87	7.067	118.5	177.3	61.79	
K88	8.615	118.3	179.0	59.28	31.27
V89	7.089	120.6	178.1	64.70	30.96
V89	$C^{\gamma 1}$: 20.81	$H^{\gamma 1}$: 0.909	$C^{\gamma 2}$: 20.63	$H^{\gamma 2}$: 0.944	
A90	7.979	120.7	180.0	54.81	18.23
A90[c]	C^{β}: 18.37	H^{β}: 1.488			
K91	7.844	117.6	180.9	59.14	31.59
E92	8.178	122.3	178.6	58.90	28.77
R93	7.776	115.3	175.0	55.63	28.28
K94	7.697	116.8	176.4	56.26	27.76
L95	7.708	120.6	177.2	56.09	42.22
L95	C^{γ}: 25.99	$C^{\delta 1}$: 23.65	$H^{\delta 1}$: 0.450	$C^{\delta 2}$: 26.27	$H^{\delta 2}$: 0.082
Q96	7.526	124.9	175.0	54.88	29.11
R97	9.039	126.0	176.8	54.92	30.73
L98	8.247	126.5	175.4	55.99	45.88
L98[a]	C^{γ}: -	$C^{\delta 1}$: -	$H^{\delta 1}$: -	$C^{\delta 2}$: -	$H^{\delta 2}$: -
Y99	6.465	110.0	173.2	54.77	37.64
I100	8.725	120.0	176.8	60.49	38.73
I100	$C^{\gamma 1}$: 26.16	$C^{\delta 1}$: 12.76	$H^{\delta 1}$: 0.671	$C^{\gamma 2}$: 16.54	$H^{\gamma 2}$: 0.702
G101	8.224	114.8	173.4	46.25	
E102	8.294	129.6	173.7	53.79	28.82
P103			175.4	61.35	31.46
S104	5.412	111.9	174.8	54.79	63.62
A105	9.211	130.2	179.4	54.39	17.32
A105[c]	C^{β}: 17.48	H^{β}: 1.284			
E106	8.731	119.8	179.3	59.58	28.02
A107	7.682	121.6	180.1	53.97	18.31
A107[c]	C^{β}: 18.45	H^{β}: 1.588			
V108	7.015	116.6	177.7	66.08	30.23
V108	$C^{\gamma 1}$: 21.84	$H^{\gamma 1}$: 0.804	$C^{\gamma 2}$: 21.68	$H^{\gamma 2}$: 1.026	
A109	8.262	121.4	181.1	54.86	16.90
A109[a]	C^{β}: -	H^{β}: -			
A110	7.607	118.8	178.9	53.62	17.55
A110[c]	C^{β}: 17.69	H^{β}: 1.446			
Q111	7.148	113.5	174.9	54.47	27.48
M112	7.882	114.7	173.3	55.21	29.33
M112[b]	C^{ϵ}: -	H^{ϵ}: -			
P113			176.7	62.13	32.23
D114	8.850	115.8	175.9	52.60	40.28
L115	-	-	174.9	52.18	
L115[a]	C^{γ}: -	$C^{\delta 1}$: -	$H^{\delta 1}$: -	$C^{\delta 2}$: -	$H^{\delta 2}$: -
I116	9.340	123.5	-	59.50	
I116[a]	$C^{\gamma 1}$: -	$C^{\delta 1}$: -	$H^{\delta 1}$: -	$C^{\gamma 2}$: -	$H^{\gamma 2}$: -
L117[a]	-	-	-	-	-
I118	-	-	174.4	59.48	41.33
I118	$C^{\gamma 1}$: 25.82	$C^{\delta 1}$: 15.24	$H^{\delta 1}$: 0.702	$C^{\gamma 2}$: 16.42	$H^{\gamma 2}$: 0.845
S119	9.575	121.6	175.7	56.60	64.57
A120	8.143	126.0	176.9	53.62	19.66
A120[c]	C^{β}: 19.79	H^{β}: 1.203			
T121	7.617	106.4	173.0	58.83	71.50
T121	$C^{\gamma 2}$: 21.42	$H^{\gamma 2}$: 0.971			
G122	7.998	104.2	177.2	43.65	
G123	-	-	174.1	45.93	
D124	8.617	116.9	176.9	51.77	39.98

Residue	$^{1}H^{N}$	^{15}N	$^{13}C'$	$^{13}C^{\alpha}$	$^{13}C^{\beta}$
S125	7.322	115.1	176.9	58.20	63.48
A126	8.837	134.9	176.7	50.47	15.95
A126[c]	C^{β}: 16.11	H^{β}: 1.429			
L127	7.353	121.0	178.9	58.11	41.58
L127	C^{γ}: 26.04	$C^{\delta 1}$: 23.90	$H^{\delta 1}$: 0.824	$C^{\delta 2}$: 24.24	$H^{\delta 2}$: 0.799
A128	8.918	121.6	178.9	54.33	17.20
A128[a]	C^{β}: -	H^{β}: -			
L129	7.776	116.8	177.0	53.31	41.45
L129	C^{γ}: 26.52	$C^{\delta 1}$: 24.97	$H^{\delta 1}$: 0.701	$C^{\delta 2}$: 22.90	$H^{\delta 2}$: 0.735
Y130	7.891	122.0	177.1	63.87	38.76
D131	9.014	119.0	178.3	57.49	38.95
Q132	7.814	118.9	179.1	58.24	28.35
L133	8.450	119.7	177.9	57.29	39.72
L133[a]	C^{γ}: -	$C^{\delta 1}$: -	$H^{\delta 1}$: -	$C^{\delta 2}$: -	$H^{\delta 2}$: -
S134	8.128	111.8	175.5	60.61	62.74
T135	6.953	111.1	175.3	62.61	68.85
T135	$C^{\gamma 2}$: 20.91	$H^{\gamma 2}$: 1.224			
I136	7.694	124.4	175.8	63.16	37.61
I136	$C^{\gamma 1}$: 26.64	$C^{\delta 1}$: 14.23	$H^{\delta 1}$: 0.796	$C^{\gamma 2}$: 17.08	$H^{\gamma 2}$: 0.780
A137	7.540	120.5	172.3	49.82	18.51
A137[c]	C^{β}: 18.57	H^{β}: 0.968			
P138			174.7	64.01	30.50
T139	7.990	122.0	173.9	60.98	70.72
T139	$C^{\gamma 2}$: 21.44	$H^{\gamma 2}$: 0.718			
L140	-	-	174.9	52.12	45.42
L140	C^{γ}: 25.86	$C^{\delta 1}$: 26.99	$H^{\delta 1}$: 0.769	$C^{\delta 2}$: 22.45	$H^{\delta 2}$: 0.452
I141	9.345	123.5	175.7	59.50	38.34
I141	$C^{\gamma 1}$: 26.14	$C^{\delta 1}$: 14.41	$H^{\delta 1}$: 0.480	$C^{\gamma 2}$: 17.27	$H^{\gamma 2}$: 0.618
I142	9.030	129.0	174.4	57.14	38.42
I142	$C^{\gamma 1}$: 26.45	$C^{\delta 1}$: 10.04	$H^{\delta 1}$: 0.632	$C^{\gamma 2}$: 17.57	$H^{\gamma 2}$: 0.753
N143	9.388	129.1	174.7	50.84	39.01
Y144	8.491	119.9	176.5	55.27	38.41
D145	8.800	125.2	176.8	54.67	42.41
D146	7.571	119.1	175.2	52.68	40.05
K147	7.018	114.1	175.0	53.38	32.23
S148	8.709	118.3	175.7	56.57	64.26
W149	8.779	121.7	179.3	59.34	26.95
Q150	8.369	124.6	178.1	60.97	25.58
S151	7.769	117.5	177.5	61.21	62.65
L152	8.460	125.2	178.7	57.70	40.72
L152[a]	C^{γ}: -	$C^{\delta 1}$: -	$H^{\delta 1}$: -	$C^{\delta 2}$: -	$H^{\delta 2}$: -
L153	8.562	119.2	179.7	58.34	40.01
L153[a]	C^{γ}: -	$C^{\delta 1}$: -	$H^{\delta 1}$: -	$C^{\delta 2}$: -	$H^{\delta 2}$: -
T154	8.004	116.3	177.2	66.66	67.83
T154	$C^{\gamma 2}$: 20.78	$H^{\gamma 2}$: 1.150			
Q155	8.230	124.5	179.2	59.02	27.65
L156	-	-	180.9	56.92	40.45
L156	C^{γ}: 26.00	$C^{\delta 1}$: 26.30	$H^{\delta 1}$: 0.686	$C^{\delta 2}$: 21.76	$H^{\delta 2}$: 0.706
G157	9.216	112.8	174.5	47.52	
E158	7.480	123.5	177.8	58.43	28.73
I159[a]	-	-	-	-	-
T160	-	-	178.3	61.28	71.05
T160	$C^{\gamma 2}$: 21.26	$H^{\gamma 2}$: 0.960			
G161	8.114	113.6	174.6	47.35	
H162	8.506	121.0	174.0	54.82	27.57
E163	10.300	123.9	180.8	60.47	27.75
K164	8.789	120.6	178.7	58.90	31.17
Q165	8.058	119.5	178.8	60.18	27.15
A166	7.873	121.1	178.0	55.60	17.40
A166[c]	C^{β}: 17.52	H^{β}: 1.298			
A167	7.642	117.9	181.5	54.42	16.95
A167[c]	C^{β}: 17.05	H^{β}: 1.416			
E168	8.230	120.1	179.6	58.92	28.82
R169[a]	-	-	-	-	-
I170	-	-	177.7	66.11	38.03
I170	$C^{\gamma 1}$: 29.25	$C^{\delta 1}$: 12.98	$H^{\delta 1}$: 0.753	$C^{\gamma 2}$: 16.43	$H^{\gamma 2}$: 0.830
A171	8.000	120.7	181.2	54.60	17.36
A171[c]	C^{β}: 17.53	H^{β}: 1.489			
Q172	8.585	120.6	179.2	58.52	27.37
F173	8.457	122.5	176.4	62.16	38.78
D174	8.771	121.0	180.3	57.49	39.45

Residue	$^{1}H^{N}$	^{15}N	$^{13}C'$	$^{13}C^{\alpha}$	$^{13}C^{\beta}$
K175	8.125	121.3	179.8	58.94	31.60
Q176	8.164	121.6	179.1	57.77	27.02
L177	8.944	125.6	178.4	59.27	39.94
L177	C^{γ}: 26.21	$C^{\delta 1}$: 26.05	$H^{\delta 1}$: 0.871	$C^{\delta 2}$: 23.94	$H^{\delta 2}$: 0.714
A178	7.690	121.5	180.6	54.71	16.97
A178[a]	C^{β}: -	H^{β}: -			
A179	7.706	120.2	180.6	54.16	17.32
A179[c]	C^{β}: 17.46	H^{β}: 1.380			
A180	8.171	121.8	179.2	54.81	17.02
A180[c]	C^{β}: 17.18	H^{β}: 1.428			
K181	8.342	118.1	178.0	59.14	32.23
E182	7.153	114.4	177.3	57.18	29.35
Q183	7.458	116.7	177.2	56.37	30.58
I184	7.723	117.8	175.2	62.24	39.03
I184	$C^{\gamma 1}$: 25.45	$C^{\delta 1}$: 14.00	$H^{\delta 1}$: 0.785	$C^{\gamma 2}$: 15.89	$H^{\gamma 2}$: 0.882
K185	8.743	127.7	175.6	53.86	30.49
L186	8.051	124.7	175.7	53.62	39.79
L186	C^{γ}: 25.58	$C^{\delta 1}$: 24.67	$H^{\delta 1}$: 0.420	$C^{\delta 2}$: 21.82	$H^{\delta 2}$: -0.208
P187[a]			-	-	-
P188			174.8	64.37	31.56
Q189	8.061	121.3	174.8	51.64	30.38
P190			175.5	62.13	34.34
V191	9.214	112.6	174.3	58.89	33.84
V191	$C^{\gamma 1}$: 21.57	$H^{\gamma 1}$: 1.100	$C^{\gamma 2}$: 18.86	$H^{\gamma 2}$: 0.706	
T192	8.462	120.7	172.3	62.42	70.76
T192	$C^{\gamma 2}$: 23.29	$H^{\gamma 2}$: 1.374			
A193	10.170	132.9	175.4	49.88	20.27
A193[c]	C^{β}: 20.46	H^{β}: 1.470			
I194	9.269	115.4	176.6	58.76	42.70
I194	$C^{\gamma 1}$: 24.46	$C^{\delta 1}$: 13.79	$H^{\delta 1}$: 0.615	$C^{\gamma 2}$: 17.93	$H^{\gamma 2}$: 0.782
V195	8.484	118.5	176.2	62.35	33.67
V195	$C^{\gamma 1}$: 20.14	$H^{\gamma 1}$: 0.926	$C^{\gamma 2}$: 20.67	$H^{\gamma 2}$: 1.102	
Y196	9.989	132.2	174.7	56.45	40.54
T197	8.262	124.9	174.3	60.12	67.75
T197	$C^{\gamma 2}$: 21.23	$H^{\gamma 2}$: 0.982			
A198	8.524	130.5	180.4	54.84	17.64
A198[c]	C^{β}: 17.73	H^{β}: 1.314			
A199	8.578	118.7	177.7	53.67	17.48
A199[c]	C^{β}: 17.61	H^{β}: 1.244			
A200	6.638	116.7	176.6	50.61	19.25
A200[c]	C^{β}: 19.35	H^{β}: 1.203			
H201	7.569	116.9	172.9	56.16	27.11
S202	7.109	110.5	171.5	55.98	65.46
A203	8.618	120.9	174.9	50.22	23.62
A203[c]	C^{β}: 23.77	H^{β}: 1.242			
N204	8.333	118.9	173.3	50.97	39.37
L205	9.265	127.2	175.7	54.30	42.92
L205	C^{γ}: -	$C^{\delta 1}$: 25.71	$H^{\delta 1}$: 0.884	$C^{\delta 2}$: 26.09	$H^{\delta 2}$: 0.827
W206	8.560	125.3	177.1	56.08	28.98
T207	8.029	112.0	176.1	59.49	67.73
T207	$C^{\gamma 2}$: 20.47	$H^{\gamma 2}$: 1.093			
P208			176.0	65.43	30.84
E209	7.612	112.3	177.1	56.59	28.79
S210	7.654	115.8	173.9	57.51	66.61
A211	8.874	125.2	180.6	54.73	17.37
A211[c]	C^{β}: 17.22	H^{β}: 1.389			
Q212	8.493	119.2	177.1	60.72	26.12
G213	8.053	107.5	175.4	46.74	
Q214	8.501	120.7	179.0	58.46	28.14
M215	7.878	119.2	177.8	59.07	31.08
M215[b]	C^{ϵ}: -	H^{ϵ}: -			
L216	7.517	115.8	179.9	57.54	38.75
L216	C^{γ}: 25.32	$C^{\delta 1}$: 25.13	$H^{\delta 1}$: 0.476	$C^{\delta 2}$: 20.04	$H^{\delta 2}$: -0.087
E217	8.377	121.0	182.2	59.52	28.18
Q218	8.464	122.3	178.1	58.53	27.88
L219	7.433	118.4	175.2	55.26	43.07
L219	C^{γ}: 26.08	$C^{\delta 1}$: 25.92	$H^{\delta 1}$: 0.712	$C^{\delta 2}$: 24.16	$H^{\delta 2}$: 0.832
G220	7.777	104.6	174.7	43.97	
F221	8.001	119.1	175.2	57.35	38.22
T222	8.961	117.6	173.9	61.17	70.56
T222	$C^{\gamma 2}$: 21.04	$H^{\gamma 2}$: 1.201			

Residue	$^{1}H^{N}$	^{15}N	$^{13}C'$	$^{13}C^{\alpha}$	$^{13}C^{\beta}$
L223	9.269	128.3	178.3	54.14	40.34
L223	C^{γ}: 27.43	$C^{\delta 1}$: 23.96	$H^{\delta 1}$: 0.787	$C^{\delta 2}$: 22.43	$H^{\delta 2}$: 0.778
A224	9.077	126.8	177.4	51.78	17.75
A224[c]	C^{β}: 17.89	H^{β}: 1.033			
K225	8.601	123.4	176.8	54.91	31.97
L226	8.634	126.2	175.5	52.80	40.46
L226	C^{γ}: 26.39	$C^{\delta 1}$: 24.93	$H^{\delta 1}$: 0.912	$C^{\delta 2}$: 23.73	$H^{\delta 2}$: 0.896
P227			176.8	62.17	31.25
A228	8.412	124.9	179.5	53.44	17.81
A228[c]	C^{β}: 17.97	H^{β}: 1.353			
G229	8.565	107.7	175.0	45.26	
L230	7.454	121.1	176.9	55.00	41.37
L230	C^{γ}: 26.29	$C^{\delta 1}$: 24.33	$H^{\delta 1}$: 0.766	$C^{\delta 2}$: 23.33	$H^{\delta 2}$: 0.738
N231	8.211	119.4	175.3	53.10	38.23
A232	8.103	124.5	178.1	52.43	18.44
A232[c]	C^{β}: 18.61	H^{β}: 1.347			
S233	8.169	115.2	175.1	58.73	63.57
Q234	8.230	122.1	176.4	55.55	28.52
S235	8.229	117.1	174.9	58.36	63.80
Q236	8.372	122.3	176.7	55.92	28.31
G237	8.381	110.4	174.1	44.94	
K238	7.968	120.5	176.6	55.80	32.21
R239	8.159	120.9	-	55.44	30.45
H240	-	-	174.8	55.19	29.05
D241	9.052	119.8	174.7	54.95	39.84
I242	7.087	115.2	175.6	58.31	42.44
I242	$C^{\gamma 1}$: 26.03	$C^{\delta 1}$: 12.67	$H^{\delta 1}$: 0.306	$C^{\gamma 2}$: 17.28	$H^{\gamma 2}$: 0.346
I243	8.746	125.1	175.3	59.56	40.03
I243	$C^{\gamma 1}$: 26.39	$C^{\delta 1}$: 12.81	$H^{\delta 1}$: 0.752	$C^{\gamma 2}$: 16.23	$H^{\gamma 2}$: 0.735
Q244	8.768	128.4	175.3	55.77	28.83
L245	8.640	125.5	176.2	53.17	43.84
L245	C^{γ}: -	$C^{\delta 1}$: 26.15	$H^{\delta 1}$: 0.811	$C^{\delta 2}$: 22.58	$H^{\delta 2}$: 0.772
G246	8.424	109.7	174.2	43.81	
G247	8.666	108.5	176.8	46.72	
E248	9.265	123.7	177.3	57.87	28.36
N249	7.963	116.7	175.5	52.94	38.68
L250	7.104	121.1	177.1	58.19	40.96
L250	C^{γ}: 26.07	$C^{\delta 1}$: 24.26	$H^{\delta 1}$: 0.772	$C^{\delta 2}$: 25.04	$H^{\delta 2}$: 0.770
A251	8.141	117.4	179.5	54.66	16.96
A251[a]	C^{β}: -	H^{β}: -			
A252	7.375	117.4	179.1	53.31	18.06
A252[c]	C^{β}: 18.19	H^{β}: 1.364			
G253	7.589	100.6	172.7	44.60	
L254	7.202	124.8	175.3	52.40	37.83
L254	C^{γ}: 26.01	$C^{\delta 1}$: 23.89	$H^{\delta 1}$: 0.607	$C^{\delta 2}$: 24.29	$H^{\delta 2}$: 0.555
N255	7.701	113.8	176.6	52.87	36.89
G256	7.856	109.1	172.2	45.01	
E257	8.443	120.1	176.9	57.19	28.79
S258	7.176	107.5	172.5	57.46	65.65
L259	8.969	124.9	173.9	53.01	44.98
L259	C^{γ}: 26.14	$C^{\delta 1}$: 24.02	$H^{\delta 1}$: 0.669	$C^{\delta 2}$: 24.53	$H^{\delta 2}$: 0.552
F260	9.295	123.7	174.2	55.91	40.85
L261	9.034	123.9	177.6	53.39	40.21
L261	C^{γ}: 27.17	$C^{\delta 1}$: 24.15	$H^{\delta 1}$: 0.490	$C^{\delta 2}$: 24.13	$H^{\delta 2}$: 0.550
F262	9.338	123.8	175.5	58.30	39.22
A263	8.902	121.9	175.3	52.95	18.78
A263[c]	C^{β}: 18.91	H^{β}: 1.734			
G264	6.746	104.5	171.1	44.76	
D265	9.052	122.3	177.3	51.11	42.13
Q266	8.277	118.4	177.6	57.93	27.52
K267	7.879	117.7	180.4	58.70	30.33
D268	7.640	121.6	177.4	57.43	40.84
A269	7.370	121.7	179.0	54.96	16.62
A269[c]	C^{β}: 16.77	H^{β}: 1.189			
D270	8.735	118.2	179.3	57.02	39.15
A271	7.579	122.9	180.8	54.36	17.38
A271[c]	C^{β}: 17.52	H^{β}: 1.696			
I272	7.340	122.3	178.3	63.09	34.39
I272	$C^{\gamma 1}$: 26.80	$C^{\delta 1}$: 9.71	$H^{\delta 1}$: -0.212	$C^{\gamma 2}$: 15.89	$H^{\gamma 2}$: 0.201
Y273	7.509	116.3	177.0	60.55	37.06
A274	7.495	118.6	177.2	51.35	18.67

Residue	^{1}H^N	^{15}N	^{13}C$'$	^{13}C$^\alpha$	^{13}C$^\beta$
A274[c]	C$^\beta$: 18.84	H$^\beta$: 1.420			
N275	7.200	119.9	175.7	50.48	37.88
P276			178.9	64.50	31.33
L277	7.777	116.7	178.0	56.01	40.46
L277	C$^\gamma$: 26.42	C$^{\delta1}$: 24.24	H$^{\delta1}$: 0.889	C$^{\delta2}$: 22.02	H$^{\delta2}$: 0.856
L278	7.485	115.1	176.6	52.58	39.70
L278	C$^\gamma$: 25.52	C$^{\delta1}$: 25.31	H$^{\delta1}$: 0.713	C$^{\delta2}$: 20.16	H$^{\delta2}$: 0.564
A279	6.665	118.6	177.7	54.40	18.85
A279[c]	C$^\beta$: 19.05	H$^\beta$: 1.276			
H280	8.337	111.6	175.5	54.81	28.83
L281	7.289	124.1	176.3	52.71	39.23
L281	C$^\gamma$: 26.20	C$^{\delta1}$: 26.27	H$^{\delta1}$: 0.958	C$^{\delta2}$: 21.61	H$^{\delta2}$: 0.806
P282			178.2	65.36	31.04
A283	7.969	116.0	179.0	54.94	18.55
A283[c]	C$^\beta$: 18.70	H$^\beta$: 0.966			
V284	6.557	115.2	180.0	64.80	31.36
V284	C$^{\gamma1}$: 20.74	H$^{\gamma1}$: 0.930	C$^{\gamma2}$: 21.74	H$^{\gamma2}$: 0.514	
Q285	8.581	121.2	178.0	58.81	28.11
N286	8.117	112.6	174.5	52.61	37.68
K287	7.724	118.5	176.1	56.85	27.46
Q288	8.895	119.7	173.7	52.28	27.67
V289	6.246	119.2	175.1	60.74	31.42
V289	C$^{\gamma1}$: 20.45	H$^{\gamma1}$: 0.352	C$^{\gamma2}$: 19.82	H$^{\gamma2}$: 0.269	
Y290	8.682	125.7	174.1	56.28	40.24
A291	9.057	126.9	178.3	50.89	18.81
A291[c]	C$^\beta$: 18.96	H$^\beta$: 1.134			
L292	8.342	120.8	175.5	54.26	41.23
L292	C$^\gamma$: 25.94	C$^{\delta1}$: 23.84	H$^{\delta1}$: -0.121	C$^{\delta2}$: 21.42	H$^{\delta2}$: 0.425
G293	7.973	107.5	177.6	44.33	
T294	8.808	117.8	176.4	64.61	67.51
T294	C$^{\gamma2}$: 22.45	H$^{\gamma2}$: 1.151			

Residue	^{1}H^N	^{15}N	^{13}C$'$	^{13}C$^\alpha$	^{13}C$^\beta$
E295	10.380	122.1	177.7	57.85	28.04
T296	7.062	103.0	173.6	61.69	68.36
T296	C$^{\gamma2}$: 21.48	H$^{\gamma2}$: 1.066			
F297	8.108	121.5	174.5	61.15	38.93
R298	7.552	116.8	176.0	53.47	31.35
L299	8.903	125.5	174.8	53.68	40.41
L299	C$^\gamma$: -	C$^{\delta1}$: 25.02	H$^{\delta1}$: 0.625	C$^{\delta2}$: 21.61	H$^{\delta2}$: 0.535
D300	7.735	124.6	173.4	51.33	42.52
Y301	7.943	118.1	175.3	61.10	38.03
Y302	7.309	112.3	180.8	61.42	37.28
S303	9.411	119.1	176.3	60.14	62.47
A304	8.860	126.9	180.4	55.31	17.12
A304[c]	C$^\beta$: 17.25	H$^\beta$: 0.840			
M305	7.346	116.6	179.3	57.19	30.38
M305[b]	C$^\epsilon$: -	H$^\epsilon$: -			
Q306	7.633	119.3	179.0	58.72	27.48
V307	-	-	-		
V307	C$^{\gamma1}$: 20.73	H$^{\gamma1}$: 0.901	C$^{\gamma2}$: 23.90	H$^{\gamma2}$: 1.170	
L308	-	-	178.7	58.07	40.53
L308[a]	C$^\gamma$: -	C$^{\delta1}$: -	H$^{\delta1}$: -	C$^{\delta2}$: -	H$^{\delta2}$: -
D309	7.984	119.1	179.6	57.28	40.11
R310	8.463	121.7	178.9	57.90	28.71
L311	8.489	119.2	178.8	57.76	41.08
L311	C$^\gamma$: 25.73	C$^{\delta1}$: 26.71	H$^{\delta1}$: 0.619	C$^{\delta2}$: 23.49	H$^{\delta2}$: 0.721
K312	7.955	116.5	178.0	58.56	31.33
A313	7.427	119.5	180.0	53.23	17.92
A313[c]	C$^\beta$: 18.05	H$^\beta$: 1.426			
L314	7.431	119.5	177.4	56.15	42.47
L314	C$^\gamma$: 25.58	C$^{\delta1}$: 24.31	H$^{\delta1}$: 0.476	C$^{\delta2}$: 21.92	H$^{\delta2}$: 0.742
F315	7.271	123.8	180.2	57.36	40.34

[a] Residue could not be observed in the experiments for assigning backbone resonances or methyl groups. [b] Methyl groups of Met cannot be assigned using our experiment. [c] The slight discrepancy between the ^{13}C$^\beta$ frequency from the backbone assignment and methyl group assignment is due to the isotope effect and is described in the Appendix of Chapter 3.

Table A2.4. Backbone and Side Chain Assignments of Holo-FepB

Residue	^{1}H^N	^{15}N	^{13}C$'$	^{13}C$^\alpha$	^{13}C$^\beta$
S12	-	-	174.7	58.08	63.81
S13	8.489	118.6	175.0	58.39	63.64
G14	8.391	111.0	173.7	44.81	
H15	8.201	119.6	174.6	55.32	29.15
I16	8.155	123.8	175.8	60.71	37.95
I16	C$^{\gamma1}$: 26.08	C$^{\delta1}$: 12.11	H$^{\delta1}$: 0.713	C$^{\gamma2}$: 16.74	H$^{\gamma2}$: 0.767
D17	8.426	124.6	175.9	54.10	40.74
D18	8.221	121.4	176.3	54.28	40.66
D19	8.280	120.8	176.3	54.36	40.61
D20	8.199	120.9	176.6	54.24	40.40
K21	8.059	121.2	176.8	55.98	31.61
H22	8.334	119.4	174.8	55.38	28.37
M23	8.289	122.1	175.7	55.21	32.19
M23[b]	C$^\epsilon$: -	H$^\epsilon$: -			
A24	8.300	125.2	177.2	51.74	18.91
A24[c]	C$^\beta$: -	H$^\beta$: 1.385			
D25	8.318	120.5	174.3	54.72	40.70
W26	7.812	120.0	174.1	54.72	30.68
P27			175.8	62.11	36.19
R28	8.726	118.0	173.5	54.39	32.30
Q29	8.544	120.7	175.4	54.11	29.83
I30	9.035	124.3	175.6	57.73	39.38
I30	C$^{\gamma1}$: 26.00	C$^{\delta1}$: 10.56	H$^{\delta1}$: 0.744	C$^{\gamma2}$: 18.05	H$^{\gamma2}$: 0.888
T31	9.040	125.3	174.3	61.59	69.87
T31	C$^{\gamma2}$: 21.13	H$^{\gamma2}$: 1.137			
D32	9.398	129.5	177.4	52.07	42.18
S33	8.268	112.1	175.6	60.28	62.68
R34	8.462	120.5	176.1	54.22	29.71

Residue	^{1}H^N	^{15}N	^{13}C$'$	^{13}C$^\alpha$	^{13}C$^\beta$
G35	7.888	109.0	171.1	44.26	
T36	8.239	116.2	173.8	62.06	69.24
T36	C$^{\gamma2}$: 21.45	H$^{\gamma2}$: 0.997			
H37	9.028	125.8	173.9	53.44	30.26
T38	9.155	121.5	174.1	62.58	69.26
T38	C$^{\gamma2}$: 21.68	H$^{\gamma2}$: 1.072			
L39	9.181	129.6	176.9	53.35	41.95
L39	C$^\gamma$: -	C$^{\delta1}$: 25.89	H$^{\delta1}$: 1.113	C$^{\delta2}$: 22.99	H$^{\delta2}$: 0.989
E40	9.208	124.4	175.5	58.74	29.78
S41	7.365	108.3	171.7	55.74	64.55
Q42	7.408	124.1	174.5	53.03	27.47
P43			176.2	63.49	
Q44	11.220	125.2	175.4	55.03	31.65
R45	10.060	125.7	174.6	54.72	32.10
I46	7.981	120.9	176.4	60.88	38.83
I46	C$^{\gamma1}$: 26.76	C$^{\delta1}$: 14.41	H$^{\delta1}$: 0.566	C$^{\gamma2}$: 15.72	H$^{\gamma2}$: 0.515
V47	-	-	174.8	60.21	32.94
V47	C$^{\gamma1}$: 22.80	H$^{\gamma1}$: 0.841	C$^{\gamma2}$: 22.52	H$^{\gamma2}$: 0.888	
S48	7.880	118.5	175.4	55.27	64.17
T49	8.324	116.9	171.3	62.11	68.49
T49	C$^{\gamma2}$: 20.70	H$^{\gamma2}$: 1.073			
S50	7.503	115.3	174.8	54.19	63.68
V51	9.426	134.8	175.1	64.96	30.97
V51	C$^{\gamma1}$: 19.38	H$^{\gamma1}$: -	C$^{\gamma2}$: 22.53	H$^{\gamma2}$: 1.685	
T52	8.163	116.2	178.9	67.53	68.29
T52	C$^{\gamma2}$: 19.17	H$^{\gamma2}$: -0.083			
L53	7.682	120.7	178.4	56.62	40.66
L53	C$^\gamma$: -	C$^{\delta1}$: 25.94	H$^{\delta1}$: 0.837	C$^{\delta2}$: 23.54	H$^{\delta2}$: 0.937

Residue	$^{1}H^{N}$	^{15}N	$^{13}C'$	$^{13}C^{\alpha}$	$^{13}C^{\beta}$
T54	7.884	116.9	174.7	66.54	
T54[a]	$C^{\gamma 2}$: -	$H^{\gamma 2}$: -			
G55	6.657	106.4	175.3	47.08	
S56	6.544	115.4	-	62.98	63.71
L57[a]	-	-	-	-	-
L58	-	-	181.1	57.02	39.83
L58	C^{γ}: -	$C^{\delta 1}$: 26.36	$H^{\delta 1}$: 0.104	$C^{\delta 2}$: 21.90	$H^{\delta 2}$: 0.580
A59	7.789	121.5	178.3	54.51	18.07
A59[a]	C^{β}: -	H^{β}: -			
I60	-	-	172.7	59.51	36.59
I60	$C^{\gamma 1}$: 22.94	$C^{\delta 1}$: 12.84	$H^{\delta 1}$: 0.620	$C^{\gamma 2}$: 17.24	$H^{\gamma 2}$: 0.713
D61	7.782	116.0	174.7	55.38	38.20
A62	7.760	118.7	176.7	49.37	17.08
A62[c]	C^{β}: -	H^{β}: 0.876			
P63			173.6	62.53	26.47
V64	8.367	123.1	174.7	57.54	32.13
V64	$C^{\gamma 1}$: 17.84	$H^{\gamma 1}$: 0.752	$C^{\gamma 2}$: 21.57	$H^{\gamma 2}$: 0.698	
I65	8.602	122.3	177.0	60.31	38.15
I65	$C^{\gamma 1}$: 25.32	$C^{\delta 1}$: 13.57	$H^{\delta 1}$: 0.790	$C^{\gamma 2}$: 17.80	$H^{\gamma 2}$: 0.870
A66	7.263	120.6	175.0	50.61	22.19
A66[c]	C^{β}: -	H^{β}: 1.114			
S67	8.573	111.8	176.4	54.52	65.33
G68	7.743	113.4	170.8	45.83	
A69	7.250	121.6	178.2	50.73	22.90
A69[c]	C^{β}: -	H^{β}: 1.416			
T70	9.220	119.0	171.2	56.63	70.80
T70[a]	$C^{\gamma 2}$: -	$H^{\gamma 2}$: -			
T71	7.577	117.9	172.2	61.68	69.40
T71	$C^{\gamma 2}$: -	$H^{\gamma 2}$: -			
P72			177.1	62.77	31.20
N73	8.349	114.9	174.2	54.09	36.54
N74	7.265	118.1	175.2	51.28	36.91
R75	7.962	112.7	177.1	58.79	30.46
V76	7.129	104.7	175.6	59.00	32.16
V76[a]	$C^{\gamma 1}$: -	$H^{\gamma 1}$: -	$C^{\gamma 2}$: -	$H^{\gamma 2}$: -	
A77	7.519	126.0	177.1	50.48	24.05
A77[c]	C^{β}: -	H^{β}: 1.119			
D78	8.644	120.5	177.9	51.28	40.63
D79	8.297	116.8	176.2	55.33	39.36
Q80	8.258	117.0	175.6	54.43	30.16
G81	7.415	105.6	173.7	44.90	
F82	8.320	122.4	-	51.64	37.04
L83	-	-	177.7	55.20	38.34
L83[a]	C^{γ}: -	$C^{\delta 1}$: -	$H^{\delta 1}$: -	$C^{\delta 2}$: -	$H^{\delta 2}$: -
R84	6.560	115.1	178.5	60.33	30.46
Q85	9.888	117.4	175.2	57.82	24.62
W86	6.392	115.1	175.7	54.15	27.56
S87	6.958	117.7	177.6	61.65	63.50
K88	8.549	117.5	179.0	59.22	31.26
V89	7.075	120.9	178.1	64.84	31.09
V89	$C^{\gamma 1}$: 20.81	$H^{\gamma 1}$: 0.906	$C^{\gamma 2}$: 20.57	$H^{\gamma 2}$: 0.848	
A90	8.157	120.3	180.2	54.86	18.42
A90[c]	C^{β}: -	H^{β}: 1.595			
K91	7.716	117.7	180.6	59.36	31.63
E92	8.259	122.3	178.6	58.94	28.83
R93	7.838	115.1	174.9	55.69	28.38
K94	7.725	117.0	176.3	56.24	27.89
L95	7.782	120.4	177.2	56.04	42.36
L95	C^{γ}: -	$C^{\delta 1}$: 23.72	$H^{\delta 1}$: 0.472	$C^{\delta 2}$: 26.50	$H^{\delta 2}$: 0.164
Q96	7.547	125.3	174.7	55.00	29.15
R97	9.066	125.7	176.7	54.77	31.03
L98	8.303	126.9	175.3	56.08	46.22
L98[a]	C^{γ}: -	$C^{\delta 1}$: -	$H^{\delta 1}$: -	$C^{\delta 2}$: -	$H^{\delta 2}$: -
Y99	6.506	109.7	173.0	54.64	37.75
I100	8.710	119.9	177.1	60.24	38.96
I100	$C^{\gamma 1}$: 26.02	$C^{\delta 1}$: 12.90	$H^{\delta 1}$: 0.681	$C^{\gamma 2}$: 16.63	$H^{\gamma 2}$: 0.731
G101	8.327	115.4	173.1	46.66	
E102	8.219	129.7	173.3	53.43	29.16
P103[a]			-	-	-
S104	5.433	112.2	174.8	54.65	64.16
A105	9.243	130.5	179.3	54.50	17.29

Residue	$^{1}H^{N}$	^{15}N	$^{13}C'$	$^{13}C^{\alpha}$	$^{13}C^{\beta}$
A105[c]	C^{β}: -	H^{β}: 1.287			
E106	8.754	119.8	179.3	59.48	28.14
A107	7.690	121.7	180.2	54.08	18.36
A107[c]	C^{β}: -	H^{β}: 1.603			
V108	7.053	116.5	177.6	66.11	30.30
V108	$C^{\gamma 1}$: 21.99	$H^{\gamma 1}$: 0.820	$C^{\gamma 2}$: 21.74	$H^{\gamma 2}$: 1.050	
A109	8.348	121.5	181.1	54.85	17.03
A109[c]	C^{β}: -	H^{β}: 1.440			
A110	7.659	118.8	178.9	53.63	17.56
A110[c]	C^{β}: -	H^{β}: 1.455			
Q111	7.166	113.5	174.9	54.51	27.48
M112	7.930	114.8	173.2	55.17	29.37
M112[b]	C^{ϵ}: -	H^{ϵ}: -			
P113			176.6	62.15	32.43
D114	8.886	115.6	-	52.60	40.10
L115[a]	-	-	-	-	-
I116[a]	-	-	-	-	-
L117[a]	-	-	-	-	-
I118	-	-	174.5	59.55	41.53
I118	$C^{\gamma 1}$: 25.89	$C^{\delta 1}$: 15.16	$H^{\delta 1}$: 0.719	$C^{\gamma 2}$: 16.34	$H^{\gamma 2}$: 0.824
S119	9.850	121.4	175.8	56.62	65.30
A120	8.350	126.7	176.7	53.91	19.53
A120[c]	C^{β}: -	H^{β}: 1.351			
T121	7.465	105.4	173.3	59.45	72.74
T121[a]	$C^{\gamma 2}$: -	$H^{\gamma 2}$: -			
G122	8.700	106.1	175.9	43.00	
G123	11.130	115.2	174.0	45.37	
D124	9.083	115.2	176.8	51.37	40.20
S125	7.314	115.8	176.1	57.97	63.46
A126	8.797	135.0	176.6	50.34	15.87
A126[c]	C^{β}: -	H^{β}: 1.421			
L127	7.438	121.2	178.7	58.03	41.96
L127	C^{γ}: -	$C^{\delta 1}$: 23.82	$H^{\delta 1}$: 0.849	$C^{\delta 2}$: 24.57	$H^{\delta 2}$: 0.857
A128	8.928	121.3	178.8	54.27	17.31
A128[c]	C^{β}: -	H^{β}: 1.378			
L129	7.757	116.8	177.0	53.24	41.56
L129	C^{γ}: -	$C^{\delta 1}$: 24.96	$H^{\delta 1}$: 0.699	$C^{\delta 2}$: 23.03	$H^{\delta 2}$: 0.729
Y130	7.915	122.0	176.9	63.78	38.91
D131	9.059	119.0	178.3	57.51	38.98
Q132	7.858	118.8	179.0	58.22	28.44
L133	8.506	119.7	177.8	57.26	39.74
L133[a]	C^{γ}: -	$C^{\delta 1}$: -	$H^{\delta 1}$: -	$C^{\delta 2}$: -	$H^{\delta 2}$: -
S134	8.154	111.7	175.4	60.63	62.45
T135	6.984	110.9	175.2	62.58	68.92
T135	$C^{\gamma 2}$: 20.92	$H^{\gamma 2}$: 1.231			
I136	7.749	124.5	175.7	63.17	37.75
I136	$C^{\gamma 1}$: 26.64	$C^{\delta 1}$: 14.29	$H^{\delta 1}$: 0.798	$C^{\gamma 2}$: 17.06	$H^{\gamma 2}$: 0.789
A137	7.574	120.5	172.2	49.79	18.47
A137[c]	C^{β}: -	H^{β}: 0.968			
P138			174.7	64.03	30.58
T139	8.051	122.2	173.7	61.01	70.67
T139	$C^{\gamma 2}$: 21.58	$H^{\gamma 2}$: 0.754			
L140	-	-	174.9	52.13	45.21
L140	C^{γ}: -	$C^{\delta 1}$: 26.98	$H^{\delta 1}$: 0.784	$C^{\delta 2}$: 22.36	$H^{\delta 2}$: 0.456
I141	9.445	123.5	175.2	59.82	38.31
I141	$C^{\gamma 1}$: 26.18	$C^{\delta 1}$: 14.17	$H^{\delta 1}$: 0.439	$C^{\gamma 2}$: 17.58	$H^{\gamma 2}$: 0.657
I142	-	-	175.2	56.96	38.73
I142	$C^{\gamma 1}$: 26.69	$C^{\delta 1}$: 9.46	$H^{\delta 1}$: 0.649	$C^{\gamma 2}$: 17.73	$H^{\gamma 2}$: 0.840
N143	9.432	127.6	174.7	52.89	39.95
Y144	9.226	117.9	176.3	54.80	39.17
D145	9.946	124.7	173.3	54.97	39.99
D146	7.390	115.0	176.0	51.74	41.21
K147	6.877	114.4	174.7	53.27	33.46
S148	8.319	115.1	175.5	55.98	64.24
W149	9.040	121.5	180.0	59.78	26.87
Q150	8.295	124.2	178.2	60.59	26.06
S151	8.071	118.9	177.9	61.12	62.39
L152	8.113	123.7	178.0	57.50	40.69
L152[a]	C^{γ}: -	$C^{\delta 1}$: -	$H^{\delta 1}$: -	$C^{\delta 2}$: -	$H^{\delta 2}$: -
L153	-	-	179.5	57.62	41.48
L153	C^{γ}: -	$C^{\delta 1}$: 23.10	$H^{\delta 1}$: 0.784	$C^{\delta 2}$: 25.80	$H^{\delta 2}$: -

Residue	$^{1}H^{N}$	^{15}N	$^{13}C'$	$^{13}C^{\alpha}$	$^{13}C^{\beta}$
T154	8.437	115.9	177.3	66.57	67.98
T154	$C^{\gamma 2}$: 20.54	$H^{\gamma 2}$: 1.131			
Q155	7.960	124.4	179.1	59.11	27.50
L156	-	-	180.8	57.20	40.03
L156	C^{γ}: -	$C^{\delta 1}$: 26.36	$H^{\delta 1}$: 0.748	$C^{\delta 2}$: 21.73	$H^{\delta 2}$: 0.729
G157	9.133	112.2	174.3	47.45	
E158	7.608	123.7	177.9	58.45	28.69
I159[a]	-	-	-	-	-
T160	-	-	178.3	61.32	70.98
T160	$C^{\gamma 2}$: 21.41	$H^{\gamma 2}$: 0.983			
G161	8.138	113.6	174.6	47.41	
H162	8.553	121.1	174.0	54.77	27.61
E163	10.280	123.6	180.7	60.31	27.86
K164	8.807	120.7	178.8	58.97	31.27
Q165	8.146	119.5	178.9	60.03	27.06
A166	7.945	121.7	178.1	55.31	17.16
A166[c]	C^{β}: -	H^{β}: 1.321			
A167	7.921	118.5	181.2	54.44	16.93
A167[a]	C^{β}: -	H^{β}: -			
E168	8.100	120.4	179.5	58.96	28.82
R169	8.016	118.7	180.2	56.81	29.11
I170	-	-	177.6	66.02	37.63
I170	$C^{\gamma 1}$: 29.40	$C^{\delta 1}$: 12.98	$H^{\delta 1}$: 0.667	$C^{\gamma 2}$: 16.40	$H^{\gamma 2}$: 0.838
A171	8.214	122.1	181.4	54.78	17.40
A171[c]	C^{β}: -	H^{β}: 1.512			
Q172	8.308	119.9	179.9	58.65	27.60
F173	8.408	121.8	176.7	61.84	39.02
D174	9.346	122.1	179.9	57.59	39.72
K175	7.675	120.0	179.6	58.94	31.75
Q176	7.342	119.8	179.0	57.25	27.18
L177	9.183	124.8	177.9	57.82	40.00
L177[a]	C^{γ}: -	$C^{\delta 1}$: -	$H^{\delta 1}$: -	$C^{\delta 2}$: -	$H^{\delta 2}$: -
A178	7.793	120.8	180.5	54.73	17.01
A178[a]	C^{β}: -	H^{β}: -			
A179	7.045	118.8	180.2	54.03	17.49
A179[c]	C^{β}: -	H^{β}: 1.415			
A180	8.124	121.2	179.7	54.60	17.42
A180[a]	C^{β}: -	H^{β}: -			
K181	8.538	117.0	178.5	59.25	31.50
E182	7.336	115.6	177.1	57.48	29.26
Q183	7.453	116.1	176.7	56.14	30.66
I184	7.647	117.5	175.4	61.99	38.96
I184	$C^{\gamma 1}$: 25.60	$C^{\delta 1}$: 13.54	$H^{\delta 1}$: 0.730	$C^{\gamma 2}$: 15.93	$H^{\gamma 2}$: 0.848
K185	8.722	128.7	175.4	53.92	31.04
L186	8.186	124.6	175.4	53.71	39.37
L186	C^{γ}: -	$C^{\delta 1}$: 23.81	$H^{\delta 1}$: 0.315	$C^{\delta 2}$: 21.88	$H^{\delta 2}$: -0.025
P187[a]			-	-	-
P188			174.7	64.09	31.71
Q189	8.111	121.0	174.6	51.78	30.31
P190			175.4	62.06	34.50
V191	9.168	113.5	174.3	58.90	33.98
V191	$C^{\gamma 1}$: 21.30	$H^{\gamma 1}$: 0.983	$C^{\gamma 2}$: 19.08	$H^{\gamma 2}$: 0.628	
T192	8.468	121.2	172.1	62.63	70.61
T192	$C^{\gamma 2}$: 23.39	$H^{\gamma 2}$: 1.382			
A193	10.080	133.0	175.6	49.82	21.15
A193[c]	C^{β}: -	H^{β}: 1.514			
I194	9.253	114.9	176.6	58.87	42.97
I194	$C^{\gamma 1}$: 24.26	$C^{\delta 1}$: 13.70	$H^{\delta 1}$: 0.633	$C^{\gamma 2}$: 17.99	$H^{\gamma 2}$: 0.796
V195	8.644	118.3	177.1	62.99	33.79
V195	$C^{\gamma 1}$: 20.48	$H^{\gamma 1}$: 1.010	$C^{\gamma 2}$: 20.77	$H^{\gamma 2}$: -	
Y196	10.570	135.0	175.3	56.44	40.57
T197	8.594	126.4	174.0	61.80	68.20
T197	$C^{\gamma 2}$: 20.88	$H^{\gamma 2}$: 1.036			
A198	8.661	131.5	180.7	55.00	17.66
A198[c]	C^{β}: -	H^{β}: 1.328			
A199	8.783	118.9	177.6	54.07	17.51
A199[c]	C^{β}: -	H^{β}: -			
A200	6.444	115.9	176.3	50.39	19.25
A200[c]	C^{β}: -	H^{β}: 1.216			
H201	7.498	116.3	172.2	56.01	26.87
S202	7.277	109.8	171.3	56.29	66.23

Residue	$^{1}H^{N}$	^{15}N	$^{13}C'$	$^{13}C^{\alpha}$	$^{13}C^{\beta}$
A203	8.168	119.0	173.9	50.49	24.47
A203[c]	C^{β}: -	H^{β}: 1.296			
N204	7.945	118.2	173.1	50.99	39.71
L205	9.257	127.5	176.1	53.93	43.45
L205	C^{γ}: -	$C^{\delta 1}$: 25.84	$H^{\delta 1}$: 0.877	$C^{\delta 2}$: 26.47	$H^{\delta 2}$: 0.855
W206	8.719	124.6	177.3	55.98	29.05
T207	8.355	113.0	175.6	59.25	68.21
T207	$C^{\gamma 2}$: 20.47	$H^{\gamma 2}$: 1.123			
P208			176.3	65.07	30.92
E209	7.645	112.3	176.3	57.85	29.41
S210	7.217	112.6	-	57.58	66.83
A211	-	-	181.7	55.24	17.16
A211[c]	C^{β}: -	H^{β}: 1.411			
Q212	8.079	120.1	177.3	61.26	25.70
G213	8.274	109.4	176.1	46.95	
Q214	8.887	120.7	179.5	59.34	27.11
M215	8.124	120.5	177.9	58.87	30.99
M215[b]	C^{ϵ}: -	H^{ϵ}: -			
L216	7.897	117.8	179.6	57.79	38.89
L216	C^{γ}: -	$C^{\delta 1}$: 25.44	$H^{\delta 1}$: -	$C^{\delta 2}$: 20.26	$H^{\delta 2}$: 0.088
E217	8.383	120.4	181.4	59.39	28.14
Q218	8.194	123.4	177.9	58.62	27.10
L219	7.662	119.0	175.3	55.41	42.69
L219	C^{γ}: -	$C^{\delta 1}$: 25.33	$H^{\delta 1}$: 0.818	$C^{\delta 2}$: 23.65	$H^{\delta 2}$: 0.806
G220	7.749	104.4	174.7	44.05	
F221	8.065	119.3	175.3	57.16	38.66
T222	8.937	117.3	173.7	61.09	70.67
T222	$C^{\gamma 2}$: 21.07	$H^{\gamma 2}$: 1.205			
L223	9.157	128.2	178.2	54.21	40.78
L223	C^{γ}: -	$C^{\delta 1}$: 24.11	$H^{\delta 1}$: 0.824	$C^{\delta 2}$: 22.94	$H^{\delta 2}$: 0.790
A224	9.000	126.7	177.3	51.68	17.86
A224[c]	C^{β}: -	H^{β}: 1.032			
K225	8.689	123.7	176.7	54.76	31.99
L226	8.713	127.3	175.5	52.77	40.76
L226	C^{γ}: -	$C^{\delta 1}$: 24.91	$H^{\delta 1}$: 0.930	$C^{\delta 2}$: 24.14	$H^{\delta 2}$: 0.915
P227			176.0	62.11	31.39
A228	8.264	123.7	179.2	52.17	18.33
A228[c]	C^{β}: -	H^{β}: 1.344			
G229	8.535	108.0	174.9	45.46	
L230	7.647	120.7	176.8	55.03	40.97
L230	C^{γ}: -	$C^{\delta 1}$: 24.83	$H^{\delta 1}$: 0.763	$C^{\delta 2}$: 23.26	$H^{\delta 2}$: 0.698
N231	8.571	122.4	174.0	52.60	37.71
A232	8.140	125.6	177.8	51.55	20.03
A232[c]	C^{β}: -	H^{β}: 1.334			
S233	8.194	116.0	174.4	57.32	63.71
Q234	8.550	123.4	178.1	54.49	28.21
S235	8.325	120.0	176.4	60.97	62.17
Q236	9.094	120.9	175.0	55.77	27.82
G237	7.799	108.5	172.7	43.81	
K238	8.182	120.4	176.3	55.88	30.72
R239	8.533	123.7	175.4	55.20	32.22
H240	10.300	118.1	174.8	56.49	29.69
D241	10.210	117.1	176.0	55.57	38.95
I242	6.539	108.4	176.8	57.50	43.94
I242[a]	$C^{\gamma 1}$: -	$C^{\delta 1}$: -	$H^{\delta 1}$: -	$C^{\gamma 2}$: -	$H^{\gamma 2}$: -
I243	8.871	124.7	175.6	59.19	39.30
I243	$C^{\gamma 1}$: 25.94	$C^{\delta 1}$: 11.41	$H^{\delta 1}$: 0.761	$C^{\gamma 2}$: 15.89	$H^{\gamma 2}$: 0.714
Q244	8.776	127.0	175.5	55.42	29.30
L245	8.479	123.0	177.1	53.26	43.21
L245	C^{γ}: -	$C^{\delta 1}$: 26.27	$H^{\delta 1}$: 0.837	$C^{\delta 2}$: 22.02	$H^{\delta 2}$: 0.761
G246	8.497	109.7	173.9	44.07	
G247	8.674	108.3	176.9	46.57	
E248	9.241	123.3	177.1	57.82	28.60
N249	7.990	116.6	175.3	52.68	38.85
L250	7.110	120.4	177.3	58.13	40.94
L250	C^{γ}: -	$C^{\delta 1}$: 24.67	$H^{\delta 1}$: 0.814	$C^{\delta 2}$: 25.23	$H^{\delta 2}$: 0.827
A251	8.288	117.5	179.4	54.77	17.01
A251[a]	C^{β}: -	H^{β}: -			
A252	7.456	117.4	179.0	53.32	18.11
A252[c]	C^{β}: -	H^{β}: 1.357			
G253	7.608	100.4	172.6	44.50	

Residue	$^{1}H^{N}$	^{15}N	$^{13}C'$	$^{13}C^{\alpha}$	$^{13}C^{\beta}$
L254	7.236	124.4	175.3	52.21	37.93
L254	C^{γ}: -	$C^{\delta 1}$: 24.08	$H^{\delta 1}$: 0.615	$C^{\delta 2}$: 24.29	$H^{\delta 2}$: 0.568
N255	7.765	114.1	176.5	52.82	36.89
G256	7.974	109.3	172.2	44.98	
E257	8.436	119.7	176.9	57.10	28.94
S258	7.227	107.7	172.4	57.41	66.22
L259	9.058	125.2	173.7	53.01	44.88
L259	C^{γ}: -	$C^{\delta 1}$: 23.93	$H^{\delta 1}$: 0.700	$C^{\delta 2}$: 24.81	$H^{\delta 2}$: 0.550
F260	9.452	124.6	174.4	55.41	41.03
L261	9.155	124.0	176.8	53.29	39.88
L261	C^{γ}: -	$C^{\delta 1}$: 24.61	$H^{\delta 1}$: 0.489	$C^{\delta 2}$: 23.96	$H^{\delta 2}$: 0.566
F262	9.439	123.0	175.4	57.46	40.14
A263	8.564	120.6	174.7	52.65	18.42
A263[a]	C^{β}: -	H^{β}: -			
G264	6.721	103.4	170.7	44.88	
D265	8.614	122.0	176.9	51.24	42.07
Q266	8.311	118.9	177.4	57.97	27.51
K267	8.111	117.2	180.2	58.95	30.49
D268	7.751	121.6	177.5	57.19	40.71
A269	7.099	121.9	178.7	54.91	16.57
A269[c]	C^{β}: -	H^{β}: 1.208			
D270	8.666	117.8	179.3	57.08	39.22
A271	7.660	122.5	180.8	54.43	17.51
A271[c]	C^{β}: -	H^{β}: 1.715			
I272	7.453	122.3	178.6	62.41	34.11
I272	$C^{\gamma 1}$: 26.44	$C^{\delta 1}$: 8.43	$H^{\delta 1}$: -0.377	$C^{\gamma 2}$: 16.00	$H^{\gamma 2}$: 0.187
Y273	7.615	116.7	176.7	60.71	37.12
A274	7.508	118.8	177.1	51.36	18.64
A274[c]	C^{β}: -	H^{β}: 1.439			
N275	7.226	119.5	177.1	50.21	37.85
P276			178.8	64.49	31.26
L277	7.768	116.7	177.8	56.00	40.32
L277	C^{γ}: -	$C^{\delta 1}$: 24.26	$H^{\delta 1}$: 0.902	$C^{\delta 2}$: 21.98	$H^{\delta 2}$: 0.866
L278	7.474	115.0	176.6	52.54	39.79
L278	C^{γ}: -	$C^{\delta 1}$: 25.34	$H^{\delta 1}$: 0.709	$C^{\delta 2}$: 20.04	$H^{\delta 2}$: 0.578
A279	6.684	118.4	177.6	54.41	18.98
A279[c]	C^{β}: -	H^{β}: 1.299			
H280	8.371	111.6	175.4	54.72	28.93
L281	7.288	124.0	176.1	52.62	39.39
L281	C^{γ}: -	$C^{\delta 1}$: 26.39	$H^{\delta 1}$: 0.983	$C^{\delta 2}$: 21.54	$H^{\delta 2}$: 0.811
P282			178.1	65.44	31.16
A283	7.989	115.8	178.8	55.00	18.49
A283[c]	C^{β}: -	H^{β}: 0.956			
V284	6.576	114.9	180.1	64.79	31.47
V284	$C^{\gamma 1}$: 20.83	$H^{\gamma 1}$: 0.928	$C^{\gamma 2}$: 21.56	$H^{\gamma 2}$: 0.494	

Residue	$^{1}H^{N}$	^{15}N	$^{13}C'$	$^{13}C^{\alpha}$	$^{13}C^{\beta}$
Q285	8.720	121.6	177.9	58.82	28.20
N286	8.129	112.5	174.3	52.63	37.67
K287	7.809	118.3	176.1	56.79	27.54
Q288	8.934	120.0	173.6	52.29	27.46
V289	6.165	119.0	175.1	60.61	31.65
V289	$C^{\gamma 1}$: 20.46	$H^{\gamma 1}$: 0.367	$C^{\gamma 2}$: 19.78	$H^{\gamma 2}$: 0.294	
Y290	8.762	125.1	174.0	56.13	40.65
A291	9.239	126.8	178.1	50.64	18.77
A291[c]	C^{β}: -	H^{β}: 1.129			
L292	8.535	121.3	175.0	54.23	41.31
L292	C^{γ}: -	$C^{\delta 1}$: 23.80	$H^{\delta 1}$: -0.164	$C^{\delta 2}$: 21.48	$H^{\delta 2}$: 0.328
G293	7.802	106.7	177.2	44.09	
T294	8.737	117.2	175.7	65.03	68.24
T294	$C^{\gamma 2}$: 22.15	$H^{\gamma 2}$: 1.138			
E295	9.286	121.3	174.8	56.05	26.54
T296	6.719	103.4	173.3	60.64	68.36
T296	$C^{\gamma 2}$: 21.71	$H^{\gamma 2}$: 0.955			
F297	7.897	124.0	175.8	59.96	40.06
R298	8.079	114.6	174.9	51.20	31.49
L299	9.402	123.6	173.2	52.33	41.55
L299	C^{γ}: -	$C^{\delta 1}$: 25.26	$H^{\delta 1}$: 0.622	$C^{\delta 2}$: 22.76	$H^{\delta 2}$: 0.564
D300	7.663	122.9	174.5	51.18	43.93
Y301	7.073	115.9	174.5	60.67	39.47
Y302	7.807	113.4	181.1	60.36	36.53
S303	8.937	115.1	177.3	59.05	63.41
A304	8.935	127.1	180.3	55.11	16.48
A304[a]	C^{β}: -	H^{β}: -			
M305	7.118	115.0	179.5	57.05	30.31
M305[b]	C^{ϵ}: -	H^{ϵ}: -			
Q306	7.045	118.3	179.3	58.61	27.53
V307	8.449	121.4	177.5	66.20	30.37
V307	$C^{\gamma 1}$: 20.57	$H^{\gamma 1}$: 0.894	$C^{\gamma 2}$: 23.98	$H^{\gamma 2}$: 1.048	
L308	7.685	118.9	178.4	58.17	40.59
L308[a]	C^{γ}: -	$C^{\delta 1}$: -	$H^{\delta 1}$: -	$C^{\delta 2}$: -	$H^{\delta 2}$: -
D309	7.441	118.0	179.2	57.26	39.97
R310	8.104	121.7	178.6	57.39	28.63
L311	8.588	118.7	178.7	57.65	40.94
L311	C^{γ}: -	$C^{\delta 1}$: 26.85	$H^{\delta 1}$: 0.746	$C^{\delta 2}$: 23.11	$H^{\delta 2}$: -
K312	7.897	116.6	177.7	58.50	31.47
A313	7.377	119.7	179.7	53.03	18.05
A313[c]	C^{β}: -	H^{β}: 1.444			
L314	7.422	119.3	177.2	56.06	43.06
L314	C^{γ}: -	$C^{\delta 1}$: 24.55	$H^{\delta 1}$: 0.494	$C^{\delta 2}$: 21.81	$H^{\delta 2}$: 0.746
F315	7.478	123.5	-	57.50	40.60

[a] Residue could not be observed in the experiments for assigning backbone resonances or methyl groups. [b] Methyl groups of Met cannot be assigned using our experiment. [c] The slight discrepancy between the $^{13}C^{\beta}$ frequency from the backbone assignment and methyl group assignment is due to the isotope effect and is described in the Appendix of Chapter 3.

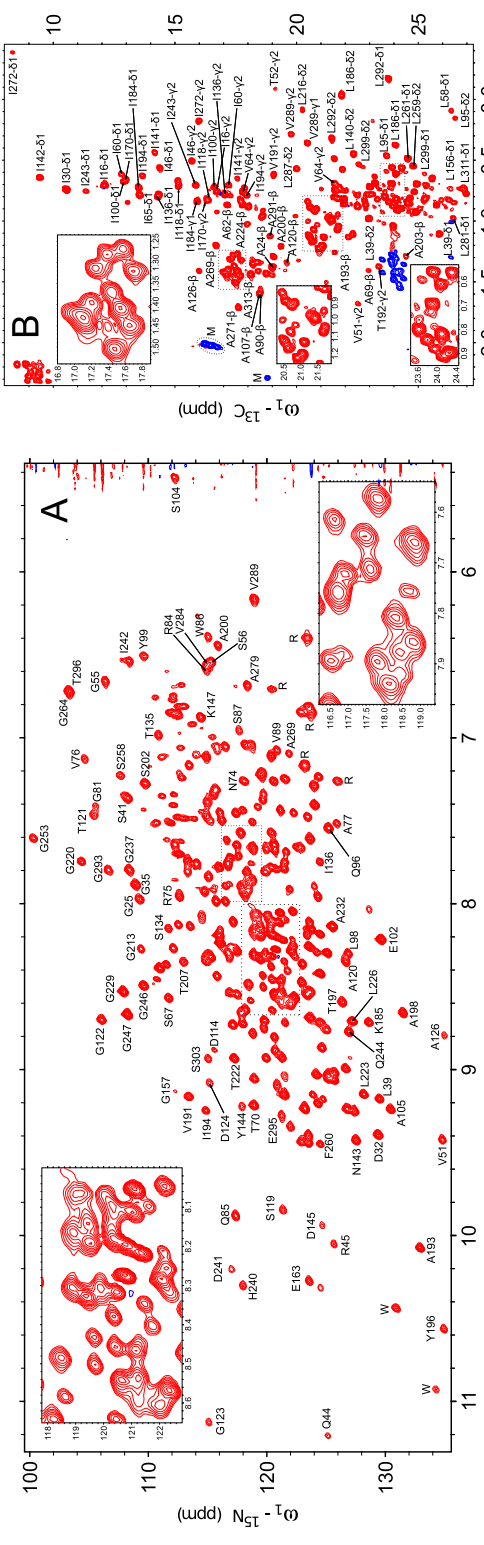

Figure A2.1. [^{1}H– ^{15}N]-TROSY-HSQC (panel A) and the CHD$_2$-detected CT-[^{1}H– ^{13}C]-HSQC (panel B) spectrum of holo-FepB recorded at 25 °C. (A) A subset of the peaks assigned to backbone residues are labeled by their one-letter amino acid code and residue number; signals originating from Arg side chain NH_2, and cross-peaks tentatively assigned to Trp side chain indole protons are designated by R and W, respectively. The weak signal pairs near 110–114 (^{15}N) and 6.6–7.5 (^{1}H) ppm originate from Gln/Asn side chain NH_2 and have not been assigned. (B) A subset of the cross-peaks of the stereospecifically assigned methyl groups are labeled by their one-letter amino acid code and residue number, negative (dark) signals between 1.2 and 1.5 ppm originate from CHD methylene groups and (unassigned) signals belonging to Met are designated by M.

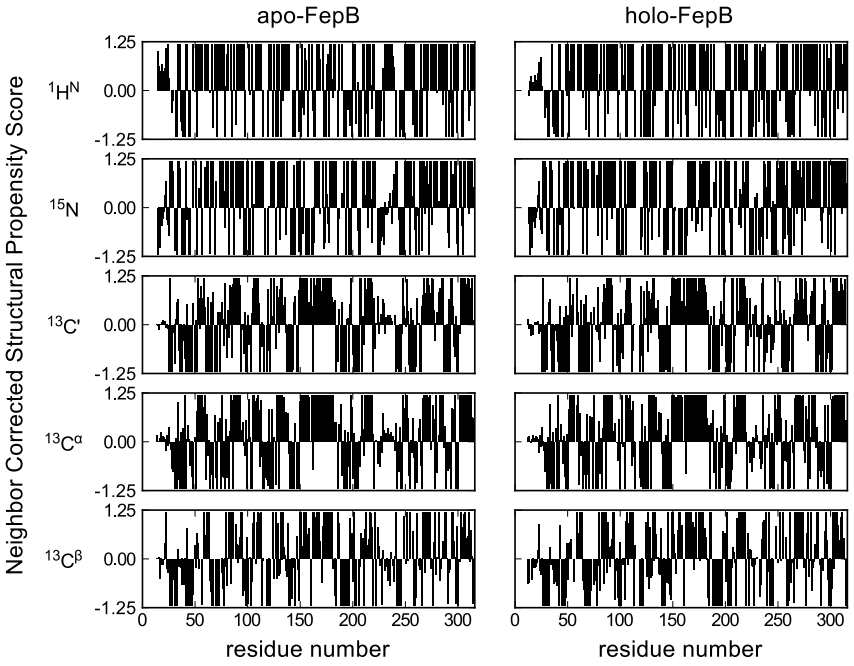

Figure A2.2. Neighbor corrected structural propensity (ncSP) score of apo- (left) and holo-FepB (right) calculated per nucleus.

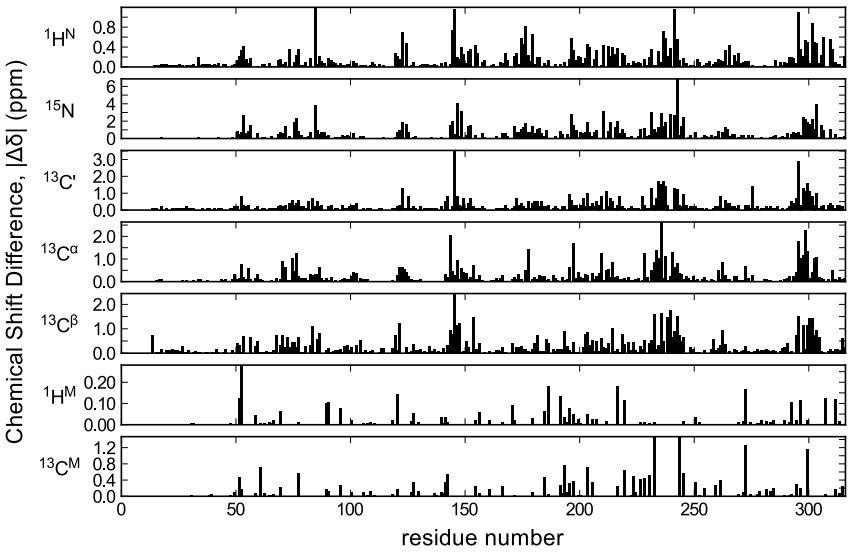

Figure A2.3. Chemical changes upon binding of the GaEnt ligand to FepB as experienced by the individual nuclei.